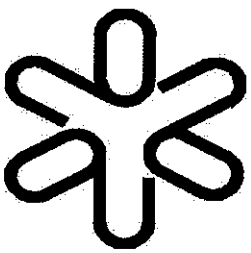

Instituto de Física
Universidade de São Paulo

Three Flavor Long-wavelength Vacuum Oscillation Solution to the Solar Neutrino Problem

Gago, A.M.[1,2], Nunokawa, H.[3], Zukanovich Funchal, R.[1]

[1] *Departamento de Física Nuclear, Instituto de Física, Universidade de São Paulo, São Paulo, Brazil*

[2] *Sección Física, Departamento de Ciencias, Pontificia Universidad Católica del Perú, Lima, Perú*

[3] *Instituto de Física Gleb Wataghin, Universidade Estadual de Campinas, UNICAMP, São Paulo, Brazil*

Publicação IF - 1414/2000

UNIVERSIDADE DE SÃO PAULO
Instituto de Física
Cidade Universitária
Caixa Postal 66.318
05315-970 - São Paulo - Brasil

IFUSP-DFN/00-053

Three Flavor Long-wavelength Vacuum Oscillation Solution to the Solar Neutrino Problem

A. M. Gago[1,2] *, H. Nunokawa[3] †, and R. Zukanovich Funchal[1] ‡

[1] *Instituto de Física, Universidade de São Paulo*
C. P. 66.318, 05315-970 São Paulo, Brazil

[2] *Sección Física, Departamento de Ciencias, Pontificia Universidad Católica del Perú*
Apartado 1761, Lima, Perú

[3] *Instituto de Física Gleb Wataghin, Universidade Estadual de Campinas, UNICAMP*
13083-970 – Campinas, Brazil.

Abstract

We investigate to what extent the presence of a third neutrino can affect and modify the long-wavelength vacuum oscillation solution to the solar neutrino problem. Assuming that the smaller mass squared difference that can induce such oscillations, Δm^2_{12}, is in the range $10^{-11} - 10^{-8}$ eV^2 and the larger one, Δm^2_{23}, in the range relevant to atmospheric neutrino observations, we analyze the most recent solar neutrino data coming from Homestake, SAGE, GALLEX and Super-Kamiokande experiments in the context of three neutrino generations. We include in our vacuum oscillation analysis the MSW effect in the Sun, which is relevant for some of the parameter space scrutinized. We have also performed, as an extreme exercise, the fit without Homestake data. While we found that the MSW effect basically does not affect the best fitted parameters, it significantly modifies the allowed parameter space for Δm^2_{12} larger than $\sim 5 \times 10^{-10}$ eV^2, in good agreement with the result obtained by A. Friedland in the case of two generations. Although the presence of a third neutrino does not essentially improve the quality of the fit, the solar neutrino data alone can give an upper bound on θ_{13}, which is constrained to be less than $\sim 60°$ at 95 % C.L.

Typeset using REVTEX

*E-mail: agago@charme.if.usp.br

†E-mail: nunokawa@ifi.unicamp.br

‡E-mail: zukanov@charme.if.usp.br

I. INTRODUCTION

The solar neutrino problem (SNP) [1] seems now to be established as a definite signal of non-standard neutrino properties by the four first generation solar neutrino experiments, Homestake [2], Kamiokande [3], GALLEX [4], SAGE [5] and by the new generation higher statistic solar neutrino experiment, Super-Kamiokande [6], which has strengthened the existence of the SNP. Astrophysical explanations of the SNP, which requires significant deviation from the standard solar model (SSM) [7,8], are highly excluded with the current solar neutrino data [9]. Moreover, there is an excellent agreement between the sound velocity predicted by the SSM and that obtained from the recent helioseismological observations [10], which supports the rigidness of the SSM.

Albeit electron neutrinos, produced in the Sun, most certainly vanish on their way to the Earth, which is the dynamical origin of the process that promotes their disappearance is yet to be completely clarified. It has been discussed that the SNP can be nicely explained by the simplest extension of the standard electroweak model which invokes neutrino mass and flavor mixing [11]. The most plausible solutions in this context are provided either by the matter enhanced resonant neutrino conversion, the MSW effect [12], or by the vacuum oscillation [13] with a typical wavelength as long as the Sun-Earth distance [14]. Recent detailed analyses and discussions of the solar neutrino data based on these mechanisms, *i.e.* the MSW and long-wavelength vacuum oscillation (LVO) solutions, in the context of two neutrino generations, can be found, in Refs. [15,16] and Refs. [15,17], respectively. Earlier detailed analyses, prior to the Super-Kamiokande experimental results, can be found in Refs. [18,19]. Discussions on other possibilities to explain the SNP by invoking more exotic properties such as neutrino magnetic moment, flavor changing interactions or violation of the equivalence principle, can be found, for example, in Ref. [20].

Although it seems at present that pure $\nu_\mu \to \nu_\tau$ oscillations in vacuum are quite enough to account for the atmospheric neutrino anomaly [21,22], the possibility of having contributions from non-negligible $\nu_\mu \to \nu_e$ oscillations is still not discarded [23,24], even after taking into account the constraints coming from the CHOOZ reactor experiment [25]. Moreover, the existence of at least three neutrino flavors, which is one of the most impressive results from the LEP experiments [26,27], makes it unavoidable to try to understand neutrino oscillations in a full three generation scenario.

In the framework of three generations of massive neutrinos subjected to flavor mixing, one has to deal, in general, with six variables to study the neutrino oscillation phenomena, namely, three mixing angles, θ_{12}, θ_{23}, θ_{13} and one CP violating phase δ, which relate mass and flavor eigenstates, and two (independent) mass squared differences, which can be chosen as $\Delta m^2_{12} \equiv m^2_2 - m^2_1$ and $\Delta m^2_{23} \equiv m^2_3 - m^2_2$. If we assume that the smaller mass squared difference, defined as Δm^2_{12}, is in the range relevant to solar neutrino oscillation, *i.e.* $\Delta m^2_{12} \sim 10^{-11} - 10^{-8}$ eV^2 in the case of the LVO solution or $\Delta m^2_{12} \sim 10^{-8} - 10^{-5}$ eV^2 in the case of the MSW solution, and the larger one, Δm^2_{23}, is in the range relevant to the atmospheric neutrino observations, *i.e.* $\Delta m^2_{23} \sim 10^{-3} - 10^{-2}$ eV^2, only three of these variables become significant in practice to the solar neutrino investigation: θ_{12}, θ_{13} and Δm^2_{12} [28–30].

Under such assumption, a detailed analysis of the three flavor LVO solution to the SNP was performed in Ref. [31] in which the best fit was obtained when θ_{13} is zero, this angle

being constrained to be less than $\sim 30^\circ$ at 95 % C.L. by the solar neutrino data alone. The authors of Ref. [31] have in addition taken into account the atmospheric neutrino results, and found that the combined three generation fit does not lead to an allowed region appreciably different from the one obtained by performing two separate effective two-neutrino fits to the solar and atmospheric neutrino data. See, for instance, Ref. [32] for earlier discussions on the three flavor LVO solution to the SNP.

On the other hand, a detailed three flavor analysis of the MSW solution to the SNP was performed in Ref. [33] and not long ago its updated version has been reported in Ref. [34]. The best fit obtained by this study permitted to constrain $\theta_{13} \lesssim 55^\circ - 60^\circ$ at 95 % C.L. by the solar neutrino data on its own, without taking into account the atmospheric neutrino observations [21] or the CHOOZ result [25]. More recently, a complete analysis considering four neutrinos, three active and one sterile, was performed in the context of both MSW as well as LVO oscillation solutions [35], and bounds on mixing angles were again obtained solely by the solar neutrino data.

In this same spirit we re-examine and update in this paper the long-wavelength vacuum oscillation solution to the SNP in the two generation as well as in the three generation frameworks. In this study, we do not take into account the constraints on θ_{13} coming from the Super-Kamiokande atmospheric neutrino observations [21] nor by the CHOOZ reactor experiment [25], whose combination gives an upper bound on θ_{13} corresponding to $\sin^2\theta_{13} \lesssim$ few % [23,24]. The main idea of this paper is to constrain θ_{13} by LVO and the solar neutrino data alone, as it has already been done for the atmospheric neutrino [23,24] as well as for the MSW solar neutrino solutions [34].

Moreover, we investigate the effect of taking the ^{8}B neutrino flux as known only up to a normalization factor, $f_{\rm B}$, renormalizing, in this case, the ^{7}Be flux accordingly, assuming the solar temperature power-law [36]. Finally, we also perform an extreme check analysis by neglecting completely the solar neutrino rate measured by the Homestake experiment, as considered, for instance, in Ref. [37], on the account of it being the only experiment which has not been calibrated.

There are new ingredients we include in this work, which were not considered in previous analyses of the three flavor LVO solution. We extend the analysis to mass squared differences up to 10^{-8} eV^2 in order to cover the whole relevant LVO parameter space. Above this value the oscillation probability of solar neutrinos essentially does not depend on the distance between the Sun and the Earth as discussed in Ref. [38], and we do not regard such case as a LVO solution to the SNP. Thereby, we include in our estimations the MSW effect in the Sun in the context of the LVO solution, whose importance was first pointed out in Ref. [39] for $\Delta m^2_{12}/E$ larger than 3×10^{-10} eV^2/MeV. The relevance of the MSW effect in determining the LVO allowed parameter space has been recently discussed in Ref [40]. Due to the presence of matter effect, we cover the whole relevant range of mixing angle $0 \leq \theta_{12} \leq \pi/2$ [40] in contrast to the range usually considered ($0 \leq \theta_{12} \leq \pi/4$) for the LVO solution.

We have used in our analysis the most recent solar neutrino data from the four solar

neutrino experiments[1] : the total rates measured by the Homestake chlorine (Cl) detector [2], by the GALLEX [4] and SAGE [5] gallium (Ga) detectors, which are summarized in Table I, as well as all the observations performed by the high-statistics Super-Kamiokande (SK) water Cherenkov detector (total rate, energy spectrum and zenith angle dependence) [6]. The pioneering Homestake experiment which has its energy threshold at $E_\nu = 0.814$ MeV [1] is mostly sensitive to ^{8}B neutrinos ($\sim$ 76 % of the total contributions), and also can detect ^{7}Be neutrinos ($\sim$ 15 %). The gallium detectors have their threshold at $E_\nu = 0.233$ MeV [1] and are sensitive to *pp* ($\sim$ 54 %), ^{7}Be ($\sim$ 27 %), and also to ^{8}B neutrinos ($\sim$ 10 %). Super-Kamiokande which has its energy threshold at $E_e = 5.5$ MeV, where E_e is the total energy of the recoil electron, is only sensitive to ^{8}B neutrinos[2].

This paper is organized as follows. In Sec. II we present the oscillation formalism we will use to pave the way to the two and three neutrino generation analysis of the data. In Sec. III we present and discuss the general features of our data analysis. In Sec. IV we revise and update the two-generation LVO solution also including the MSW effect in the Sun. In Sec. V we extend the analysis to three-generation neutrino oscillation taking into account the MSW effect. In Sec. VI we examine the seasonal effect that can be expected at SK, Borexino and KamLAND experiments for the best fitted parameters of the LVO solutions we found. In Sec. VII we discuss the LVO solution with two and three neutrino flavors disregarding the chlorine data. Finally we draw our conclusions in Sec. VIII.

II. OSCILLATION FORMALISM

In this section we describe the framework we will use in the scope of this paper.

A. Two Flavor Case

For the two generation case in which ν_e is mixed only with ν_μ (the same argument holds also for the case of $\nu_e - \nu_\tau$ mixing), the evolution equation of neutrino traveling through matter can be written as

$$i\frac{d}{dx}\begin{bmatrix}\nu_e\\ \nu_\mu\end{bmatrix} = \begin{bmatrix} V_e(x) & \frac{1}{2}\Delta_{12}\sin 2\theta_{12} \\ \frac{1}{2}\Delta_{12}\sin 2\theta_{12} & \Delta_{12}\cos 2\theta_{12}\end{bmatrix}\begin{bmatrix}\nu_e\\ \nu_\mu\end{bmatrix}, \tag{1}$$

where $\Delta_{12} \equiv \Delta m^2_{12}/2E$, with the mass squared difference of the two neutrino mass eigenstates $\Delta m^2_{12} = m^2_2 - m^2_1$, E is the neutrino energy, θ_{12} is the mixing angle,

---

[1]For the sake of simplicity, we have not included the data from the Kamiokande experiment [3], which can be justified by the fact that its result is consistent with that of SK and its errors are much larger than that of the SK experiment.

[2]In this work, we do not take into account the possible enhancement of *hep* neutrinos [41] in the SK spectrum analysis since the current SK data do not seem to decisively conclude on the necessity of such enhancement.

$$V_e(x) \equiv \sqrt{2} G_F N_e(x) \simeq 7.6 \times 10^{-14} \times \left[\frac{N_e}{1 \text{ mol/cc}}\right] \text{ eV}^2, \tag{2}$$

is the matter potential for ν_e with G_F and N_e being the Fermi constant and the electron number density, respectively.

This equation, in the case of vacuum ($V_e = 0$), simplifies to lead to the well known formula for the ν_e survival probability,

$$\begin{aligned} P_{2\text{g,vac}}(\nu_e \to \nu_e) &= 1 - \sin^2 2\theta_{12} \sin^2 \left(\frac{\Delta_{12}}{2} L\right) \\ &= 1 - \sin^2 2\theta_{12} \sin^2 \left(1.27 \left[\frac{\Delta m^2_{12}}{\text{eV}^2}\right] \left[\frac{\text{MeV}}{E}\right] \left[\frac{L}{\text{m}}\right]\right), \end{aligned} \tag{3}$$

where L is the distance traveled by the neutrino. It is clear that the probability $P_{2\text{g,vac}}$ is invariant under the transformation $\Delta m^2_{12} \to -\Delta m^2_{12}$ as well as $\theta_{12} \to \frac{\pi}{2} - \theta_{12}$ and therefore, in vacuum it is sufficient to assume $\Delta m^2_{12} > 0$ and $0 \leq \theta_{12} \leq \frac{\pi}{4}$ to account for all physical situations.

From Eq. (3) we can estimate the vacuum oscillation length as,

$$\begin{aligned} L_{\text{osc}} = \frac{4\pi E}{\Delta m^2_{12}} &\simeq 2.47 \times 10^{10} \left[\frac{E}{1 \text{ MeV}}\right] \left[\frac{10^{-10}\text{eV}^2}{\Delta m^2_{12}}\right] \text{m} \\ &\simeq 0.165\, L_0 \left[\frac{E}{1 \text{ MeV}}\right] \left[\frac{10^{-10}\text{eV}^2}{\Delta m^2_{12}}\right], \end{aligned} \tag{4}$$

where $L_0 \equiv 1$ AU $\simeq 1.496 \times 10^{11}$ m, is the astronomical unit, namely, the mean Earth-Sun distance.

If matter is present, the physics described by the neutrino evolution given in Eq. (1) is not invariant under either transformation $\Delta m^2_{12} \to -\Delta m^2_{12}$ or $\theta_{12} \to \frac{\pi}{2} - \theta_{12}$. However, we can show that the physical consequence of Eq. (1) is invariant under the transformation $\theta_{12} \to \pi - \theta_{12}$ as well as $(\Delta m^2_{12}, \theta_{12}) \to (-\Delta m^2_{12}, \frac{\pi}{2} - \theta_{12})$. Therefore, in order to cover all the possible physically meaningful parameter region we can assume [33,34],

$$\Delta m^2_{12} > 0, \quad 0 \leq \theta_{12} \leq \frac{\pi}{2}. \tag{5}$$

This is the range we consider in this work.

In principle, neutrinos on their way from the interior of the Sun to the detector on the Earth can be influenced by the solar as well as by the Earth matter potentials.

Let us initially consider what can happen in the Sun. In Fig. 1(a) we show the iso-survival probability contours of ν_e at the solar surface as a function of $\Delta m^2_{12}/E$ and $\sin^2\theta_{12}$ for pure vacuum oscillation, ignoring the matter effect, assuming that neutrinos are created in the solar center. In Fig. 1(b) we show the same type of contours but taking into account the matter effect. The probabilities were obtained by numerically integrating Eq. (1), using the electron number density one can find in Ref. [42], again assuming that neutrinos are created in the center of the Sun.

From these two plots, we immediately see that the probability at the solar surface can be significantly different for these two cases if $\Delta m^2_{12}/E \geq$ few $\times 10^{-10}$ eV^2/MeV. Therefore,

one can not disregard the matter influence in the ν_e survival probability calculation for values of $\Delta m^2_{12}/E$ in this range. For smaller values of $\Delta m^2_{12}/E$ the oscillation effect is small and the survival probabilities are ~ 1, in both cases. For $\Delta m^2_{12}/E \sim \mathcal{O}(10^{-9})$ eV^2/MeV or smaller, the rôle of the solar matter is to suppress oscillations, as $\Delta m^2_{12}/E$ increases the MSW resonance effect comes into play and strong conversion can occur. We note that for values of $\Delta m^2_{12} \gtrsim 10^{-9}$ eV^2, the MSW conversion can be significant for lower energy neutrinos, such as *pp* and ^{7}Be ones, but it will be very weak for most of the ^{8}B neutrinos. In fact, we can see from Fig. 1 (b), that even for $\Delta m^2_{12} = 10^{-8}$ eV^2, the highest value considered in this work, if we take $E \sim 10$ MeV, the typical ^{8}B neutrino energy relevant for SK, the survival probability of ν_e at the solar surface is very close to one. This implies that at such high energies, neutrinos exit from the Sun essentially as ν_e.

Let us now examine what happens in the Earth. For the averaged electron number density found in the Earth's mantle ($N_e \sim 2$ mol/cc) or core ($N_e \sim 5$ mol/cc), the matter potential V_e is always much larger than Δ_{12}, unless Δm^2_{12} is very close to 10^{-8} eV^2 for the lowest energy (*i.e. pp*) neutrinos (see Eq. (2)), leading to a strong suppression of the effective mixing angle in the Earth matter. This implies that no appreciable $\nu_{\mu,\tau} \to \nu_e$ (or $\nu_e \to \nu_{\mu,\tau}$) re-generation effect can occur in the Earth, since this can promote, at the most, a few % change in the probability for a very limited range of mixing parameters ($\Delta_{12} \sim 10^{-7}$ eV^2/MeV and large θ_{12}). Hence, in this work we only take into account the MSW effect in the Sun and neglect it completely in the Earth.

After accounting for the MSW effect in the Sun, the ν_e survival probability at the Earth given in Eq. (3) is modified as follows [39],

$$\begin{aligned} P_{2g}(\nu_e \to \nu_e) = & \cos^2\theta_{12}|A_{\nu_1}(R_\odot)|^2 + \sin^2\theta_{12}|A_{\nu_2}(R_\odot)|^2 \\ & + \sin 2\theta_{12}|A_{\nu_1}(R_\odot)A_{\nu_2}(R_\odot)|\cos\left(\Delta_{12}L + \beta\right), \end{aligned} \tag{6}$$

where $A_{\nu_1}(R_\odot)$ and $A_{\nu_2}(R_\odot)$ are respectively the amplitudes of the neutrino state to be found in the mass eigenstate ν_1 and ν_2 at the solar surface, L is the distance between the solar surface and the detection point, and $\beta \equiv \mathrm{Arg}[A_{\nu_1}(R_\odot)A^*_{\nu_2}(R_\odot)]$ corresponds to the phase developed between ν_1 and ν_2 after the neutrinos pass the resonance point until they reach the solar surface. We remark that for the values of Δm^2_{12} we are interested in this work, in the region where ν_e's are created, typically $r \lesssim 0.3R_\odot$, because of the condition $V_e \gg \Delta_{12}$, they essentially coincide with the mass eigenstate $\nu_1 (\sim \nu_e)$, and no oscillation occurs within this region. Hence the final probability amplitudes $A_{\nu_1}(R_\odot)$ and $A_{\nu_2}(R_\odot)$ as well as β do not depend on the exact production point, allowing us to assume that all neutrinos are created in the solar center [39].

The probability in Eq. (6) can be rewritten in terms of the flavor amplitudes as,

$$\begin{aligned} & P_{2g}(\nu_e \to \nu_e) \\ & = |A_{\nu_e}(R_\odot)|^2\left[1 - \sin^2 2\theta_{12}\sin^2\left(\frac{\Delta_{12}}{2}L\right)\right] + |A_{\nu_x}(R_\odot)|^2\sin^2 2\theta_{12}\sin^2\left(\frac{\Delta_{12}}{2}L\right) \\ & - \sin 2\theta_{12}|A_{\nu_e}(R_\odot)A_{\nu_x}(R_\odot)|\left[2\cos 2\theta_{12}\sin^2\left(\frac{\Delta_{12}}{2}L\right)\cos\beta' - \sin\left(\Delta_{12}L\right)\sin\beta'\right], \end{aligned} \tag{7}$$

where $A_{\nu_e}(R_\odot)$ and $A_{\nu_x}(R_\odot)$ are respectively the probability amplitudes of the neutrino to be found in the state ν_e and ν_x (x $= \mu, \tau$) at the solar surface and $\beta' \equiv \mathrm{Arg}[A_{\nu_1}(R_\odot)A^*_{\nu_2}(R_\odot)]$,

is the phase difference developed in the flavor basis corresponding to the one we have in Eq. (6) between the mass eigenstates, namely, β. We note that the following relation holds.

$$|A_{\nu_e}(R_\odot)|^2 = \cos^2\theta_{12}|A_{\nu_1}(R_\odot)|^2 + \sin^2\theta_{12}|A_{\nu_2}(R_\odot)|^2 + \sin 2\theta_{12}|A_{\nu_1}(R_\odot)A_{\nu_2}(R_\odot)|\cos\beta. \quad (8)$$

In this work, we first compute the values of $A_{\nu_e}(R_\odot)$ and $A_{\nu_x}(R_\odot)$ by numerically integrating the neutrino evolution equation in Eq. (1) with the solar electron density taken from Ref. [42] and then compute the final probability at the Earth by using the expression in Eq. (7). We take into account the effect due to the eccentricity of the Earth orbit around the Sun by taking the time average over one year of the probability using the time dependent distance $L(t)$,

$$L(t) = L_0\left[1 - \epsilon\cos\left(2\pi\frac{t}{T}\right)\right] + \mathcal{O}(\epsilon^2), \quad (9)$$

where $L_0 = 1$ AU, $\epsilon = 0.0167$ is the orbit eccentricity and $T =$ one year. We neglect the correction terms of $\mathcal{O}(\epsilon^2)$.

Following Ref. [40], we restrict the range of Δm^2 from 10^{-11} to 10^{-8} eV^2. One can easily estimate from Eqs. (3) and (4), that for the typical energy of ^{8}B neutrinos, ~ 10 MeV, in order to have appreciable oscillation effects for solar neutrinos, the Δm^2_{12} value must be larger than of the order $\sim 10^{-11}$ eV^2. This sets our lower limit on Δm^2_{12}.

It is known (see, for *e.g.* , Ref. [40]) that if Δm^2_{12} is larger than $\sim 10^{-8}$ eV^2, the final ν_e survival probability at the Earth, averaged over the neutrino energy, would not practically depend on the precise value of the Sun-Earth distance since the variation in the probability due to the energy spread is large enough, even for ^{7}Be neutrinos, to average out the vacuum oscillation effect. Since we do not regard such a case as a LVO solution, this sets our upper limit on Δm^2_{12}. Also, to cover values of Δm^2_{12} up to 10^{-8} eV^2 means to examine the effect of the solar matter on the LVO solution to the SNP whose relevance was already discussed in Refs. [39,40].

B. Three Flavor Case

For the case when we consider three flavor mixing, the evolution equation of neutrinos in matter can be written as,

$$i\frac{d}{dx}\begin{bmatrix}\nu_e\\ \nu_\mu\\ \nu_\tau\end{bmatrix} = \left\{\begin{bmatrix}V_e(x) & 0 & 0\\ 0 & 0 & 0\\ 0 & 0 & 0\end{bmatrix} + U\begin{bmatrix}0 & 0 & 0\\ 0 & \Delta_{12} & 0\\ 0 & 0 & \Delta_{13}\end{bmatrix}U^\dagger\right\} \times \begin{bmatrix}\nu_e\\ \nu_\mu\\ \nu_\tau\end{bmatrix}, \quad (10)$$

where $\Delta_{ij} \equiv \frac{\Delta m^2_{ij}}{2E}$ and we take the representation of the Maki-Nakagawa-Sakata (MNS) [11] mixing matrix U which is the leptonic analog of the Cabbibo-Kobayashi-Maskawa (CKM) matrix in the quark sector [43] as,

$$U = e^{i\lambda_7\theta_{23}}e^{i\lambda_5\theta_{13}}e^{i\lambda_2\theta_{12}}. \quad (11)$$

Explicitly [3],

$$U = \begin{bmatrix} c_{12}c_{13} & s_{12}c_{13} & s_{13} \\ -s_{12}c_{23} - c_{12}s_{23}s_{13} & c_{12}c_{23} - s_{12}s_{23}s_{13} & s_{23}c_{13} \\ s_{12}s_{23} - c_{12}c_{23}s_{13} & -c_{12}s_{23} - s_{12}c_{23}s_{13} & c_{23}c_{13} \end{bmatrix}, \tag{12}$$

where λ_i are the SU(3) Gell-Mann's matrices and $c_{ij} = \cos\theta_{ij}$, $s_{ij} = \sin\theta_{ij}$. We assume Δm^2_{13} to be in the range $\sim 10^{-3} - 10^{-2}$ eV^2, which is consistent with atmospheric neutrino observations [22]. Because of this assumption, the relation V_e, $\Delta_{12} \ll \Delta_{23} \sim \Delta_{13}$ holds.

In this case, Δ_{13} is the dominant term in the Hamiltonian matrix and this leads to the decoupling of ν_3 from the remaining two states. This means that the oscillation which is driven by the Δ_{13} term can be simply averaged out in the final survival probability of electron neutrinos at the Earth, $P_{3g}(\nu_e \to \nu_e)$, yielding the relation [28,29],

$$P_{3g}(\nu_e \to \nu_e) = \sin^4\theta_{13} + \cos^4\theta_{13} \cdot P_{2g}(\tilde{\nu}_e \to \tilde{\nu}_e), \tag{13}$$

where $P_{2g}(\tilde{\nu}_e \to \tilde{\nu}_e)$ is defined as the survival probability of the following effective two generation system [28,30,29],

$$i\frac{d}{dx}\begin{bmatrix} \tilde{\nu}_e \\ \tilde{\nu}_\mu \end{bmatrix} = \begin{bmatrix} \cos^2\theta_{13} \cdot V_e(x) & \frac{1}{2}\Delta_{12}\sin 2\theta_{12} \\ \frac{1}{2}\Delta_{12}\sin 2\theta_{12} & \Delta_{12}\cos 2\theta_{12} \end{bmatrix} \begin{bmatrix} \tilde{\nu}_e \\ \tilde{\nu}_\mu \end{bmatrix}, \tag{14}$$

where $\tilde{\nu}_\alpha$ $(\alpha = e, \mu, \tau)$ is defined as,

$$\begin{bmatrix} \tilde{\nu}_e \\ \tilde{\nu}_\mu \\ \tilde{\nu}_\tau \end{bmatrix} = e^{-i\lambda_5\theta_{13}} e^{-i\lambda_7\theta_{23}} \begin{bmatrix} \nu_e \\ \nu_\mu \\ \nu_\tau \end{bmatrix}. \tag{15}$$

We compute $P_{2g}(\tilde{\nu}_e \to \tilde{\nu}_e)$ by using the expression in Eq. (7) just by replacing the solar electron density as $N_e(r) \to \cos^2\theta_{13} \cdot N_e(r)$.

We note that we have three independent parameters Δm^2_{12}, θ_{12} and θ_{13} which can be fitted or constrained by the experimental data. Regarding θ_{13}, it is clear that the probability in Eq. (13) is invariant under $\theta_{13} \to \pi - \theta_{13}$ allowing us to restrict the range of θ_{13} to $0 \leq \theta_{13} \leq \pi/2$. As for Δm^2_{12} and θ_{12}, we again consider the range given in Eq. (5) for the case of two generations, since the same argument discussed in the previous subsection also holds for $P_{2g}(\tilde{\nu}_e \to \tilde{\nu}_e)$.

III. DATA ANALYSIS

The general idea is to perform a χ^2 analysis to fit the oscillation free parameters (θ_{12} and Δm^2_{12}, in the case of two generations, and θ_{12}, θ_{13} and Δm^2_{12} in the case of three generations)

---

[3]Here we neglect the possible CP violating phase since this phase will not affect the ν_e survival probability, even if we take into account the next-to-leading order corrections in electroweak interactions [44].

with observed experimental data. We investigate in addition the effect of having an extra normalization factor $f_{\rm B}$ for the ^{8}B neutrino flux, which is in this case assumed to be free. In what follows we will give explicit definitions of the χ^2 for the solar rates, the SK recoil-electron spectrum, the SK zenith angle distribution as well as the combination, to be used in our analysis.

A. Calculation of the rates

We calculate, for the two (three) generation framework, our theoretical predictions for the measured solar neutrino rates as a function of the two (three) mixing parameters for the gallium and chlorine experiments by folding the neutrino oscillation probability P_{2g} (P_{3g}) with interaction cross section and the six solar neutrino fluxes corresponding to each reaction, *pp*, *pep*, ^{7}Be, ^{8}B, ^{13}N and ^{15}O as predicted by the standard solar model of Bahcall and Pinsonneault [7] (BP98 SSM). Other minor sources such as ^{17}F, *hep* and, for the gallium experiment, ^{7}Be neutrinos with smaller energy ($E = 0.383$ MeV), are not considered for simplicity. For gallium and chlorine experiments, we use the neutrino absorption cross sections found in Ref. [42] and for the SK experiment, we use the new calculation of $\nu_e, \nu_{\mu,\tau}$ scattering cross section on electrons which take into account radiative corrections [45].

In this case the expected event rate for Ga and Cl detectors that should be compared to experimental data is :

$$R_{\rm x}^{\rm theo} = C_{\rm x} \int dE \sigma_{\rm x}(E) \langle P_{\rm n}(E) \rangle \left(f_{\rm B} \phi_{\rm B}(E) + f_{\rm Be} \phi_{\rm Be}(E) + \sum_{\rm j} \phi_{\rm j}(E) \right), \qquad (16)$$

where x=Ga,Cl, n=2g,3g, $\phi_{\rm B}(E)$, $\phi_{\rm Be}(E)$ and $\phi_{\rm j}(E)$ with j=*pp*, *pep*,^{13}N and ^{15}O are the neutrino fluxes as a function of the neutrino energy taken from Ref. [7], and $C_{\rm x}$ is some normalization constant determined in such a way that $R_{\rm x}^{\rm theo}$ is given in Solar Neutrino Unit (SNU). The numbers $f_{\rm B}$ and $f_{\rm Be}$ are respectively the normalization constants for the ^{8}B and the ^{7}Be neutrino fluxes, $f_{\rm B} = f_{\rm Be} = 1$ corresponds to the BP98 SSM values. Here $\langle P_{\rm n} \rangle$ means that the probability has been averaged on the neutrino path length to take into account the eccentricity of the Earth orbit around the Sun, after we have computed the probability as in Eq. (7), for two generations, or as in Eq. (13), for three generations, with the solar matter effect included. The integral above was performed starting at the energy threshold of each experiment.

In our calculations, we have also included the effect due to the thermal broadening of about 1 keV of the ^{7}Be line [46] when computing the capture rate by performing an extra average over the ^{7}Be neutrino energy profile given in Ref. [46]. This is pertinent for large values of Δm^2_{12} as discussed, for *e.g.* , in Refs. [47,40].

When $f_{\rm B}$ is taken to be free we assume the power-law relationship between the ^{8}B and ^{7}Be fluxes, given by $\phi^{^7{\rm Be}} = (\phi^{^8{\rm B}})^{10/24}$ [36], in order to renormalize the ^{7}Be flux by a factor $f_{\rm Be}$ as

$$f_{\rm Be} = f_{\rm B}^{10/24}. \qquad (17)$$

For the SK experiment, the expected solar neutrino event rate, normalized by the BP98 SSM prediction, is given by,

$$R_{\rm SK}^{\rm theo} = \frac{f_{\rm B}\int dE_e \int dE'_e\, h(E'_e,E_e)\int dE_\nu \phi_{\rm B}(E_\nu)\left(\frac{d\sigma_{\nu_e}}{dE'_e}\langle P_{\rm n}(E_\nu)\rangle + \frac{d\sigma_{\nu_{\rm x}}}{dE'_e}[\,1-\langle P_{\rm n}(E_\nu)\rangle\,]\right)}{\int dE_e \int dE'_e\, h(E'_e,E_e)\int dE_\nu \phi_{\rm B}(E_\nu)\frac{d\sigma_{\nu_e}}{dE'_e}}, \tag{18}$$

where E_e is the observed recoil electron energy, E'_e is the true recoil electron energy, $h(E'_e,E_e)$ is the electron energy resolution function taken from Ref. [48] and $d\sigma_{\nu_e}/dE'_e$, $d\sigma_{\nu_{\rm x}}/dE'_e$ are $\nu_e - e$ and $\nu_{\rm x} - e\,({\rm x}=\mu,\tau)$ scattering cross sections taken from Ref. [45]. In the integral above we have used 6.5 MeV as the energy threshold for SK.

The definition of the $\chi^2_{\rm rates}$ function to be minimized is the same as the one used in Ref. [49] which essentially follows the prescription given in Ref. [50]. Explicitly,

$$\chi^2_{\rm rates} = \sum_{\rm x,y}(R_{\rm x}^{\rm theo} - R_{\rm x}^{\rm obs})\sigma_{\rm xy}^{-2}(R_{\rm y}^{\rm theo} - R_{\rm y}^{\rm obs}), \tag{19}$$

where x(y) runs through four solar neutrino experiments, Homestake, SAGE, GALLEX and Super-Kamiokande, the theoretical predictions $R_{\rm x(y)}^{\rm theo}$ are given in Eqs. (16) and (18) and the experimental values $R_{\rm x(y)}^{\rm obs}$ are given in Table I. The error matrix $\sigma_{\rm xy}$ contains the theoretical and experimental uncertainties according to Ref. [49] where theoretical uncertainties are taken from the ones given by the BP98 SSM [7].

B. Calculation of the SK recoil-electron Spectrum

For the spectrum shape analysis we first define the following quantity,

$$S_{\rm i}^{\rm theo} \equiv \frac{\int_{E_{\rm i}^{\rm min}}^{E_{\rm i}^{\rm max}} dE_e \int dE'_e\, h(E'_e,E_e)\int dE_\nu \phi_{\rm B}(E_\nu)\left(\frac{d\sigma_{\nu_e}}{dE'_e}\langle P_{\rm n}(E_\nu)\rangle + \frac{d\sigma_{\nu_{\rm x}}}{dE'_e}[\,1-\langle P_{\rm n}(E_\nu)\rangle\,]\right)}{\int_{E_{\rm i}^{\rm min}}^{E_{\rm i}^{\rm max}} dE_e \int dE'_e\, h(E'_e,E_e)\int dE_\nu \phi_{\rm B}(E_\nu)\frac{d\sigma_{\nu_e}}{dE'_e}}, \tag{20}$$

where $E_{\rm i}^{\rm min}$ and $E_{\rm i}^{\rm max}$ are the minimum and maximum observed recoil electron energy in the i-th bin, starting at the 5.5 MeV threshold for the SK detector. In total we have 18 bins taken at 0.5 MeV intervals, except for the last bin which includes all the contribution above 14 MeV.

The definition of the $\chi^2_{\rm spec}$ function to be minimized is the same as the one used in Ref. [16], that is,

$$\chi^2_{\rm spec} = \sum_{\rm i,j=1,18}(\alpha S_{\rm i}^{\rm theo} - S_{\rm i}^{\rm SK})\sigma_{\rm ij}^{-2}(\alpha S_{\rm j}^{\rm theo} - S_{\rm j}^{\rm SK}), \tag{21}$$

where σ_{ij} were computed as prescribed in Ref. [16] and S_i^{SK} are the experimental points whose numerical values are graphically reproduced from Ref. [6]. The extra normalization parameter α, which is always taken to be free in our analysis, is introduced because here we are only interested in fitting the shape of the spectrum. Moreover when we combine with the rates, it allows us to avoid double counting the information already taken into account in the rate analysis.

For the SK spectrum analysis, as a good approximation, we simply assume that neutrinos exit from the Sun as pure ν_e and use the vacuum probability formula in Eq. (3), for two generation, or in Eq. (13), for three generation, in this latter case removing from our expression the Sun matter effect. This is well justified by the discussion we presented in section II A.

C. Calculation of the zenith angle dependence

We define the $\chi^2_{\rm zenith}$, for the zenith angle dependence, as follows,

$$\chi^2_{\rm zenith} = \sum_{i=1,6} \frac{(\beta Z_i^{\rm theo} - Z_i^{\rm obs})^2}{\sigma^2_{Z,i}}, \tag{22}$$

where $Z_i^{\rm theo}$ is the i-th bin theoretical expectation, $Z_i^{\rm obs}$ is the i-th bin observed value, with 5 night bins and 1 day bin which are graphically reproduced from Ref. [6] and β is a free normalization constant introduced for the same reasons as in the case of the spectrum analysis. As the LVO solution does not imply in practice any zenith angle distortion of the data, this will simply provide an extra global constant that will increase the final combined $\chi^2_{\rm min}$. It is important to remark that this global constant will only affect the quality of the combined fit, bearing no influence on the computed allowed region. We obtained $\chi^2_{\rm zenith} = 6.6$ with $\beta = 0.48$ for the zenith angle distribution.

D. Combined Analysis

Finally the combined χ^2 to be minimized is simply defined as the sum of the individual ones:

$$\chi^2_{\rm comb} = \chi^2_{\rm rates} + \chi^2_{\rm spec} + \chi^2_{\rm zenith}. \tag{23}$$

E. Definitions of the confidence levels and $N_{\rm DOF}$

Using the χ^2 functions defined in the previous subsections, for the two generation analysis where we have only two mixing parameters, $(\Delta m^2_{12}, \theta_{12})$, we use the condition $\chi^2 = \chi^2_{\rm min} + \Delta\chi^2$ where $\Delta\chi^2 = 4.61$, 5.99 and 9.21 for 90, 95 and 99 % C.L., respectively, in order to determine the allowed parameter space. On the other hand, for the three generation analysis, in order to constrain the parameter space spanned by three variables $(\Delta m^2_{12}, \theta_{12},$

θ_{13}), we determine the iso-confidence level surface by the condition $\chi^2 = \chi^2_{\rm min} + \Delta\chi^2$ where $\Delta\chi^2 = 6.25$, 7.82 and 11.36 for 90, 95 and 99 % C.L., respectively, as in Ref. [34].

We note that in this work, we always determine the values of $\chi^2_{\rm min}$ within the range $10^{-11}{\rm eV}^2 < \Delta m^2_{12} < 10^{-8}{\rm eV}^2$ and therefore, do not take into consideration the region relevant for MSW solutions [15,16]. This means that in this work, "*a priori*" we assume that LVO is the solution to the solar neutrino problem, so adopting a different criteria than other authors, see for *e.g.* Ref. [35], to draw the C.L. contours.

Here, we also describe how we compute the number of degrees of freedom $N_{\rm DOF}$ which is relevant to determine the goodness of fit (or C.L.). We compute $N_{\rm DOF}$ as follows,

$$N_{\rm DOF} \equiv N_{\rm data} - N_{\rm param} - N_{\rm norm} \ , \tag{24}$$

where $N_{\rm data}$ is the number of the data points we use in each analysis, $N_{\rm param}$ is the number of mixing parameters to be constrained, two or three depending on the number of neutrino generations considered, and $N_{\rm norm}$ is the number of extra free normalization factors we introduced in the analysis, *i.e.* f_B in Eqs. (16) and (18), α in Eq. (21) and β in Eq. (22).

IV. RESULTS WITH THE TWO GENERATION SCHEME

In this section we discuss our results for the analysis of the solar neutrino data in the context of two generations.

A. Results with fixed $f_{\rm B}$

We first present the case when we fix $f_{\rm B} = 1$, therefore $f_{\rm Be} = 1$. This corresponds to use the BP98 SSM flux values. To demonstrate the influence of the solar matter in the computed allowed regions, we will show here our results without and with the MSW effect in the Sun.

In Figs. 2(a),(b) and (c) we show the allowed region in $\sin^2\theta_{12} - \Delta m^2_{12}$ parameter space, for the rates, spectrum and combined analysis, respectively, without taking into account any possible influence of the solar matter, hence all the plots are symmetric with respect to $\sin^2\theta_{12} = 0.5$ because of the invariance of the pure vacuum probability under the transformation $\theta_{12} \to \pi/2 - \theta_{12}$.

In Figs. 3(a) and (b) we show the allowed region in $\sin^2\theta_{12} - \Delta m^2_{12}$ parameter space, for the rates and combined analysis, respectively, taking into account the MSW effect. As expected we see that in this case the shape of the allowed region is not symmetric with respect to $\sin^2\theta_{12} = 0.5$, for $\Delta m^2_{12} \gtrsim 5 \times 10^{-10}$ eV^2, in good agreement with the results obtained in Ref. [40]. No spectrum analysis with the solar matter effect was performed since we have checked that the results are essentially the same as the one presented in Fig. 2(b). This is because of the fact that nearly all neutrinos that are relevant to SK exit from the Sun as pure ν_e and so we can simply use the vacuum oscillation formulas as a very good approximation (see the discussions in section II A).

The values of the $\chi^2_{\rm min}$, the best fitted parameters, the number of degrees of freedom, $N_{\rm DOF}$, as well as the goodness of the fit, the C.L. in %, for the above discussed situations are shown in Table II.

As far as the best fit points are concerned, the MSW effect in the sun is not important as it does not affect their values. In fact we have two best fit points localized at a position almost exactly symmetric with respect to $\sin^2\theta_{12} = 0.5$. We note that our global best fit point for the combined analysis agree well with that found in Ref. [35].

Comparing the region allowed by the spectrum at 90 % C.L., given in Fig. 2 (b), with the one allowed by the rates at the same C.L., given in Fig. 3 (a), we can see that the region favored by the total rates are disfavored by the spectrum information. Due to such disagreement between the total rates and the SK spectrum, in the combined analysis we obtained two kinds of solutions, one which explains better the spectrum, at $\Delta m^2_{12} \sim 4\times10^{-10}$ eV^2 or larger, where we obtained our global best and another one which explain better rates, at $\Delta m^2_{12} \sim 6 \times 10^{-11}$ eV^2.

This incompatibility makes the quality of the combined fit of the two generation LVO solution worse than that of the MSW solution.

B. Results with arbitrary $f_{\rm B}$

For the case where we consider $f_{\rm B}$ as a free parameter we also show the results of the analysis without matter in Figs. 4(a) and (b) and with matter in Figs. 5(a) and (b), for the rates and combined analysis, respectively. We note that the spectrum result is the same as the one in Fig. 2(b), since the extra normalization factor α introduced in our $\chi^2_{\rm spec}$ definition in Eq. (21) is treated independently of $f_{\rm B}$.

Again, the values of the $\chi^2_{\rm min}$ as well as of the best fitted parameters can be found in Table II. In comparison to the fixed $f_{\rm B}$ case, the fit for the rates is substantially improved and the allowed parameter region became somewhat larger. The other qualitative features mentioned in the previous subsection remain unchanged. Nevertheless the combined fit essentially was not improved by this extra freedom (see Table II).

V. RESULTS WITH THE THREE GENERATION SCHEME

In this section we discuss our results for the analysis of the solar neutrino data in the context of three neutrino generations. Here we will always present the results taking into account the solar matter effect.

A. Results with fixed $f_{\rm B}$

As for the two generation case we first consider $f_{\rm B}$ as fixed to be 1. In Fig. 6 we show the regions, in $\sin^2\theta_{12} - \Delta m^2_{12}$ parameter space, allowed by the rates for different values of $\sin^2\theta_{13}$. In each plot of Fig. 6 we are presenting a *cut* of the allowed parameter space in three generations, that is, we show the allowed region in the $\sin^2\theta_{12} - \Delta m^2_{12}$ plane for a

given value of $\sin^2\theta_{13}$, which means that the $\chi^2_{\rm min}$ value is common for all the plots shown. We found that for the rates the best fit occurs when $\sin^2\theta_{13} = 0$.

We note that, as in the case of the two generation analysis, the allowed regions that appear in the plots are asymmetric for $\Delta m^2_{12} \gtrsim 5 \times 10^{-10}$ eV^2 because of the matter effect in the Sun. Moreover, there is a tendency that the matter influence will gradually start to be important at smaller values of Δm^2_{12} as $\sin^2\theta_{13}$ increases. We can understand this by recalling that the effective potential here has been rescaled by $\cos^2\theta_{13}$ (see Eq. (14)). which means that as $\sin^2\theta_{13}$ increases, the potential decreases and can start to be relatively relevant for lower values of Δm^2_{12}.

In Fig. 7 the regions, in $\sin^2\theta_{12} - \Delta m^2_{12}$ parameter space, allowed by the spectrum for different values of $\sin^2\theta_{13}$ are displayed. Since we have used the vacuum oscillation formulas in our spectrum calculation, the allowed regions are symmetric with respect to $\sin^2\theta_{12} = 0.5$. Again, as in the case of the rates analysis, we found the best fit at $\sin^2\theta_{13} = 0$. We note that although the best fit occurs when $\theta_{13} = 0$, the region excluded by the spectrum data become smaller as θ_{13} increases. This can be qualitatively understood from the fact that the energy dependence of the probability becomes weaker as θ_{13} increases (see Eq. (13)) and consequently, the spectrum become flatter, which is consistent with the present SK data.

In Fig. 8 we plot the combined allowed region for rates and spectrum, for fixed $f_{\rm B} = 1$. The values we have obtained for the best fitted parameters and $\chi^2_{\rm min}$ as well as the estimated C.L. of the fit are presented in Table II. We have found that for the combined analysis, the best fit occurs when $\sin^2\theta_{13} = 0.05$. Notwithstanding, a small difference in χ^2 such as $\chi^2_{\rm min}(\theta_{13} = 0) - \chi^2_{\rm min}(\theta_{13} = 0.05) \simeq 0.3$ clearly bears no real statistical significance to the preferred non-zero θ_{13}.

Finally we plot in Fig. 9 the spectrum calculated for the best fitted parameters for the rates, spectrum and combined analysis, for fixed values of $\sin^2\theta_{13}$, as well as the SK experimental data points. Here some comments are in order. One of the features of the total rate analysis is that several "local" best fit points, which are rather comparable in terms of χ^2 values, exist. For $\theta_{13} = 0$ we found the best fit at $(\Delta m^2_{12}, \sin^2\theta_{12}) = (9.1\times10^{-11}$ eV^2, $0.27/0.73)$. We have noticed that as we increase the value of θ_{13} these points do not always remain as best fit points but always remain as local best. Moreover, such two symmetric (with respect to $\theta_{12} = 45°$) best fit points move smoothly toward the direction of $\theta_{12} = 0$ and $\theta_{12} = 90°$. The fitted spectrum curves for the rates, shown in Fig. 9, are, strictly speaking, indicating the "evolution" of the spectrum shape of these "best fit points" as θ_{13} increases.

We see that the best fit parameters for the rates do not produce a spectrum shape which is consistent with the SK data for lower values of $\sin^2\theta_{13}$, but the combined fit, which is dominated by the spectrum weight in the χ^2 is in fairly good agreement with the data.

B. Results with arbitrary $f_{\rm B}$

The same plots as in Fig. 6 and Fig. 8 are presented for the rates in Fig. 10 and the combined analysis in Fig. 11, respectively, when we considered $f_{\rm B}$ to be free. We do not show the spectrum allowed region in this case, since it is the same as the one shown in Fig. 7. From these plots, we can remark some interesting features. Comparing Figs. 6 and 10 or Figs. 8 and 11, we can see that for smaller values of θ_{13}, the area of the allowed region

becomes somewhat larger if f_B is taken as free, whereas for larger values of θ_{13}, there is a opposite tendency, *i.e.* the area becomes somewhat smaller if f_B is taken as free. In order to understand this behavior, we plot in Fig. 12, $\chi^2 - \chi^2_{\rm min}$ for the rates as a function of $f_{\rm B}$ for various values of θ_{13}. From this plot, we can see that as θ_{13} becomes larger the allowed values of $f_{\rm B}$ become more restricted, eventually, narrower than the range allowed by the BP98 SSM, $0.58 < f_{\rm B} < 1.57$ at 3 σ [7]. Therefore, for larger values of θ_{13}, letting $f_{\rm B}$ free, and consistently switching off the theoretical uncertainties of the ^{8}B flux, makes the allowed region smaller than the case with $f_{\rm B} = 1$.

As in the case with $f_{\rm B} = 1$, we also show in Fig. 13 the calculated spectrum for the best fitted parameters for the rates, spectrum and combined analysis, for various values of $\sin^2\theta_{13}$, as well as the SK experimental data points. The results are very similar to the case with $f_{\rm B} = 1$.

C. Constraining θ_{13}

The values of the $\chi^2_{\rm min}$ as well as of the best fitted parameters for all the above cases are shown in Table III. The combined χ^2 value includes $\chi^2_{\rm zenith}$ as for the two generation case.

To illustrate the effect of the presence of the third neutrino in the χ^2, we plot in Fig. 14 the values of $\Delta\chi^2 \equiv \chi^2 - \chi^2_{\rm min}$ as a function of $\sin^2\theta_{13}$ for the case of $f_{\rm B} = 1$ (fixed). From this plot, we see that there is a general tendency that the fit become worse as θ_{13} increases, although we note that there is a local minimum for the fit with the rates and the combined data at $\sin^2\theta_{13} \sim 0.62$. We also see that $\Delta\chi^2$ for the rates increases more rapidly than that for the spectrum. This can be understood as follows.

As pointed out in Ref. [32], naively, the fit for the rates is expected to become worse as θ_{13} increases since any energy dependence in the probability will become weaker (see Eq. (13)) and thus, in general, the larger the value of θ_{13}, the similar will become the suppressions for all the solar neutrinos, leading to a gradually stronger inconsistency with the observed total rates.

On the other hand, as we have already mentioned in the previous subsection A, the loss of energy dependence will not compromise so much the fit for the spectrum data since the observed spectrum shape is consistent with a flat one.

Finally, from Fig. 14, we can conclude that the solar neutrino data alone give the upper bound $\theta_{13} \lesssim 60^\circ$ at 95 % C.L. It is interesting to observe that this limit is quite similar to the one obtained in the case of a three flavor MSW solution to the SNP [34].

VI. PREDICTIONS FOR SEASONAL VARIATIONS

In this section we discuss, in view of our previous presented results, possible seasonal variations that could be measured by the current Super-Kamiokande detector, as well as by the future Borexino [51] and KamLAND [52] experiments, which will be sensitive to ^{7}Be neutrinos. It is clear that because of the eccentricity of the Earth orbit around the Sun, solar neutrino fluxes should vary as $1/L^2$ as L varies with time. From Eq. (9) we can estimate that the flux variation in one year due to this effect is,

$$\Delta\phi_\nu \sim \Delta\left(\frac{1}{L^2}\right) \sim \frac{4\epsilon L_0}{L^3} \sim 4\epsilon\phi_\nu \sim 0.07\phi_\nu, \tag{25}$$

which implies that the solar neutrino signals could vary as much as ~ 7 % in one year.

We can see that if vacuum oscillation is assumed, "anomalous" time variation can be expected because the expressions of the probabilities in Eqs. (3),(6) and (7) also dependent on the distance L [13,53,14]. Such "anomalous" time variation is expected to be more prominent for ^{7}Be neutrinos [54]. This is because of the fact that ^{7}Be neutrinos are mono-energetic at $E = 0.862$ MeV (and also at $E = 0.383$ MeV, with much smaller flux) with $\Delta E \sim 1$ keV [47], and the oscillation probability of such neutrinos can be very sensitive to the precise value of L, in contrast to the other neutrino fluxes such as *pp* and ^{8}B where the probability for these neutrinos must be averaged out over the neutrino energy. Detailed analyses on the seasonal variations for ^{7}Be neutrinos have been performed in Refs. [48,55,38].

In Fig. 15 we plot the expected "anomalous" seasonal variation that is expected at SK for the best fitted parameters (global and local) of the two and three generation LVO solutions jointly with the observed SK data for $E_e > 11.5$ MeV. SK presents the data subtracting the expected "normal" seasonal variation due to the $1/L^2$ dependence of the flux. For this reason we have not included this extra effect in any of our curves in this section. We see that our prediction is currently consistent with the observed SK data but being the experimental statistical errors still large we can not conclude anything definite yet.

We also have computed the seasonal variation of the rate of ^{7}Be neutrinos that one can expect to be measured by the Borexino [51] and the KamLAND [52] experiments using the best fitted parameters (global and local) for the LVO solution with two and three flavors. We note that the predictions for Borexino and KamLAND we have obtained are visually indistinguishable, and therefore, we only plot the case of Borexino in Fig. 16. As we can see from the plot, large time variation is obtained, which should be observable at both of these experiments. Such drastic variation is due to the fact that the oscillation wavelength for ^{7}Be neutrinos for our best fitted value of $\Delta m^2_{12} = 4.4 \times 10^{-10}$ eV^2, is about 3 % of the mean Sun-Earth distance (see Eq. (4)), which is comparable to the Sun-Earth distance variation due to the orbit eccentricity. For Δm^2_{12} of this order, it is irrelevant to take into account the finite width of the ^{7}Be line.

Such "anomalous" seasonal variation can be a clear signature of the vacuum oscillation, which does not depend on any detail of the SSM nor on unknown experimental systematic errors [38].

VII. ANALYSIS WITHOUT CHLORINE DATA

Finally, in this section, following Refs. [37], we have further investigated the impact of removing from our analysis the chlorine data, since Homestake is the only experiment which has not been calibrated. This is certainly an extreme case but could be worthwhile to be discussed.

A. Two generation case

In Figs. 17(a) and (b) we show our results for the rates alone and for the combined analysis, respectively, in the case of two generations. We observe here that the rates alone allow for a broader range of solutions in the $\sin^2\theta_{12} - \Delta m^2_{12}$ plane, compared to Fig. 3(a) where the chlorine data was included, making it more consistent with the SK spectrum measurement. The combined analysis without chlorine data reflects this fact by allowing for larger values of Δm^2_{12} even at 90 % C.L.

The values of the $\chi^2_{\rm min}$ as well as of the best fitted parameters here are shown in Tables IV and Table V. Again the combined χ^2 value also includes $\chi^2_{\rm zenith}$. We remark that without chlorine data the quality of the combined fit improves since there are significant overlap between the allowed parameter region which give good fit to the total rates and SK spectrum. We can see this by comparing Figs. 2(b) and 17(a). This is in contrast to the case with chlorine data.

B. Three generation case

We repeat the same analysis for some non-zero values of θ_{13}. In Figs. 18(a),(b) and (c) we show our results for the rates for three flavor oscillations, for $\sin^2\theta_{13} = 0.0, 0.05$ and 0.1, respectively. In Figs. 19 we show the same plots but for the combined three flavor analysis. Again we see that if one ignores Homestake's data completely a larger range of values of Δm^2_{12} and $\sin^2\theta_{12}$ can provide a good explanation for the measured rates as well as for all the solar data combined.

In Figs. 20(a),(b) and (c) we display the spectrum calculated for the best fitted parameters at these same values of $\sin^2\theta_{13}$, as well as the data points.

VIII. DISCUSSIONS AND CONCLUSIONS

We have re-examined the status of the SNP in the light of the LVO solution, using the most recent solar neutrino data as well as the predictions of the BP98 SSM. We have analyzed the solar neutrino data in the context of two and three neutrino flavor oscillations in vacuum, extending previous analysis to covered the range $10^{-11} \leq \Delta m^2_{12} \leq 10^{-8}$ eV^2. In doing this we have included the MSW effect in the Sun, which plays a relevant rôle in the calculations when $\Delta m^2_{12}/E \geq$ few $\times 10^{-10}$ eV^2/MeV. When we have considered three neutrino generations we assumed a mass hierarchy such that Δm^2_{13} should be large enough to be relevant for the atmospheric neutrino problem.

We have found that the MSW effect in the Sun significantly modify the allowed parameter space for Δm^2_{12} larger than $\sim 5\times 10^{-10}$ eV^2 in agreement with the result obtained in Ref. [40]. We, however, found that values of the best fitted parameters are not practically affected by the presence of the solar matter effect (see Table II).

In the two generation LVO solution we found that the rates prefer lower values of Δm^2, *i.e.* $\Delta m^2_{12} \lesssim 3\times 10^{-10}$ eV^2 at 90 % C.L., while the SK electron recoil spectrum data excludes

such favored parameter region and prefers $\Delta m^2_{12} \gtrsim 4 \times 10^{-10}$ eV^2. In the combined analysis the weight of the spectrum prevails.

The disagreement between the best fitted rates and the spectrum predictions for the LVO solution in the case of two generation is, nevertheless, less striking when three neutrinos are considered. When θ_{13} is small, the picture described above applies but as θ_{13} increase the region favored by the total rates are less excluded by the spectrum data compared to the two generation case (see for *e.g.* , Fig. 6 and Fig. 7 for the case $\sin^2\theta_{13} = 0.25$). We note. however. that more statistics is needed to establish the spectral distortion in the SK recoil electron data, and to reach any definite conclusion.

We found that the fit to the total rates as well as SK spectrum are not essentially improved due to the possibility of oscillating into a third neutrino (see Fig. 14). In particular. we obtained the upper bound on θ_{13} to be less than $\sim 60^\circ$ at 95 % C.L. by the solar neutrino data alone. We should remark that this bound is substantially weaker than the bound obtained by combining the Super-Kamiokande atmospheric neutrino observations with the CHOOZ reactor experiment limit [23,24]. Hopefully future neutrino oscillation experiments at neutrino factories will be able to give a much more precise information on θ_{13} [56].

Note added: While we were completing this work, we became aware of two similar works that appeared in hep-ph [57,58].

ACKNOWLEDGMENTS

We would like to thank Pedro C. de Holanda for useful discussions. This work was supported by Fundação de Amparo à Pesquisa do Estado de São Paulo (FAPESP) and by Conselho Nacional de e Ciência e Tecnologia (CNPq).

REFERENCES

[1] J. N. Bahcall, Neutrino Astrophysics, Cambridge University Press, 1989; for a recent review see also J. N. Bahcall, hep-ex/0002018.

[2] Homestake Collaboration, K. Lande *et al.*, Astrophys. J. **496**, 505 (1998).

[3] Kamiokande Collaboration, Y. Fukuta *et al.*, Phys. Rev. Lett. **77**, 1638 (1996).

[4] GALLEX Collaboration, W. Hampel *et al.*, Phys. Lett. B **447**, 127 (1999).

[5] Sage Collaboration, J. N. Abdurashitov *et al.*, Phys. Rev. C **60**, 055801 (1999).

[6] Y. Suzuki for Super-Kamiokande Collaboration, talk given at Lepton Photon 99 conference, available at http://lp99.slac.stanford.edu/db/program.asp.

[7] J. N. Bahcall, S. Basu, and M. H. Pinsonneault, Phys. Lett. B **433**, 1 (1998); see also Ref. [42].

[8] For other SSM, see for *e.g.* , J. N. Bahcall and R. K. Ulrich, Rev. Mod. Phys. **60**, 297 (1988); V. Castellani *et al.*, Phys. Lett. B **324**, 425 (1994); J. N. Bahcall and M. H. Pinsonneault, Rev. Mod. Phys. **67**, 781 (1995); S. Turck-Chieze *et al.*, Astrophys. J. **335**, 415 (1988).

[9] See for *e.g.* , H. Minakata and H. Nunokawa, Phys. Rev. D **59**, 073004 (1999) and references therein.

[10] J. N. Bahcall, M. H. Pinsonneault, S. Basu and J. Christensen-Dalsgaard, Phys. Rev. Lett. **78**, 171 (1997).

[11] Z. Maki, M. Nakagawa, and S. Sakata, Prog. Theor. Phys. **28**, 870 (1962).

[12] S. P. Mikheyev and A. Yu. Smirnov, Sov. J. Nucl. Phys. **42**, 913 (1985); Nuovo Cimento C **9**, 17 (1986); L. Wolfenstein, Phys. Rev. D **17**, 2369 (1978).

[13] V. N. Gribov and B. M. Pontecorvo, Phys. Lett. B **28**, 493 (1969).

[14] S. L. Glashow and L. M. Krauss, Phys. Lett. B **190**, 199 (1987); V. Barger, R. J. N. Philips, and K. Whisnant, Phys. Rev. Lett. **65**, 3084 (1990).

[15] J. N. Bahcall, P. I. Krastev and A. Yu. Smirnov, Phys. Rev. D **58**, 096016 (1998); Phys. Rev. D **60**, 093001 (1999).

[16] M. C. Gonzalez-Garcia, P. C. de Holanda, C. Peña-Garay and J. W. F. Valle, Nucl. Phys. B **573**, 3 (2000).

[17] V. Berezinsky, G. Fiorentini, and M. Lissia, Astropart. Phys. **12**, 299 (2000).

[18] For earlier MSW analyses, see for *e.g.* , N. Hata and P. Langacker, Phys. Rev. D **50**, 632 (1994); G. L. Fogli and E. Lisi, Astropart. Phys. **2**, 91 (1994); J. N. Bahcall and P. I. Krastev, Phys. Rev. D **53**, 4211 (1996).

[19] For earlier LVO analyses, see for *e.g.* , Z. G. Berezhiani and A. Rossi, Phys. Rev. D **51**, 5229 (1995); P. I. Krastev and S. T. Petcov, Phys. Rev. Lett. **72**, 1960 (1994); Phys. Rev. D **53**, 1665 (1996).

[20] For recent analyses, see for *e.g.* , M. M. Guzzo and H. Nunokawa, Astropart. Phys. **12**, 87 (1999); S. Bergmann *et al.*, hep-ph/0004049; S. W. Mansour and T. K. Kuo, Phys. Rev. D **60**, 097301 (1999); A. M. Gago, H. Nunokawa and R. Zukanovich Funchal, Phys. Rev. Lett. **84** 4035 (2000), and references therein.

[21] Super-Kamiokande Collaboration, Y. Fukuda *et al.*, Phys. Lett. B **433**, 9 (1998); *ibid.* B **436**, 33 (1998); Phys. Rev. Lett. **81**, 1562 (1998). Phys. Lett. B **467**, 185 (1999).

[22] See for instance: M. C. Gonzalez-Garcia *et al.*, Phys. Rev. D **58**, 033004 (1998); M. C. Gonzalez-Garcia, H. Nunokawa, O. L. G. Peres and J. W. F. Valle.

Nucl. Phys. B **543**, 3 (1999); N. Fornengo, M. C. Gonzalez-Garcia and J. W. F. Valle, hep-ph/0002147.
[23] G. L. Fogli, E. Lisi, A. Marrone and G. Scioscia, Phys. Rev. D **59**, 033001 (1999): See also G. L. Fogli, in the Vth International Workshop on Topics in Astroparticle and Underground Physics, *TAUP ' 99*, Paris, France, September, 1999, transparencies available at http://taup99.in2p3.fr/TAUP99.
[24] O. Yasuda, *New Era in Neutrino Physics*, ed. by H. Minakata and O. Yasuda, Universal Academic Press, Tokyo, 1999, p.165; Phys. Rev. D **58**, 091301 (1998); Acta. Phys. Polon. B **30** (1999) 3089 [hep-ph/9910428].
[25] CHOOZ Collaboration, M. Apollonio *et al.*, Phys. Lett. B **420**, 397 (1998); *ibid.*, B **466**, 415 (1999).
[26] C. Caso *et al.*, Eur. Phys. J. C, **3**, 1 (1998).
[27] A. Straessner for the L3 Collaboration, talk given at the XXXVth Rencontres de Moriond, 11-18 March 2000, Les Arcs, France; available at http://moriond.in2p3.fr/EW/2000/transparencies/6_Friday/pm/Straessner/.
[28] C-S. Lim, in *Proceedings of BNL Neutrino Workshop*, p. 249, February 1987, New York. USA, Edited by M. J. Murtagh, BNL-52079, C87/02/05.
[29] G. L. Fogli, E. Lisi, and D. Montanino, Phys. Rev. D **49**, 3626 (1994); Astropart. Phys. **4**, 177 (1995).
[30] T. K. Kuo and J. Pantaleone, Phys. Rev. Lett. **57**, 1805 (1986); Phys. Rev. D **35**, 3432 (1987); Rev. Mod. Phys. **61**, 937 (1989).
[31] V. Barger and K. Whisnant, Phys. Rev. D **59**, 093007 (1999).
[32] Z. G. Berezhiani and A. Rossi, Phys. Lett. B **367**, 219 (1996).
[33] G. L. Fogli, E. Lisi, and D. Montanino, Phys. Rev. D **54**, 2048 (1996).
[34] G. L. Fogli, E. Lisi, and D. Montanino and A. Palazzo, Phys. Rev. D **62**, 013002 (2000).
[35] C. Giunti, M. C. Gonzalez-Garcia, and C. Peña-Garay, hep-ph/0001101.
[36] J. N. Bahcall and A. Ulmer, Phys. Rev. D **53**, 4202 (1996).
[37] A. de Gouvea, A. Friedland, and H. Murayama, hep-ph/0002064.
[38] A. de Gouvea, A. Friedland and H. Murayama, Phys. Rev. D **60**, 093011 (1999).
[39] J. Pantaleone, Phys. Lett. B **251**, 618 (1990).
[40] A. Friedland, hep-ph/0002063.
[41] J. N. Bahcall and P. I. Krastev, Phys. Lett. B **436**, 243 (1998); R. Escribano *et al.*, Phys. Lett. B **444**, 243 (1998); G. Fiorentini *et al.*, Phys. Lett. B **444**, 387 (1998); C. J. Horowitz, Phys. Rev. C **60**, 022801 (1999).
[42] J. N. Bahcall's web site at http://www.sns.ias.edu/~jnb/.
[43] N. Cabbibo, Phys. Rev. Lett. **10**, 531 (1963); M. Kobayashi and T. Maskawa, Prog. Theor. Phys. **49**, 652 (1973).
[44] H. Minakata and S. Watanabe, Phys. Lett. B **468**, 256 (1999).
[45] J. N. Bahcall, M. Kamionkowski, and A. Sirlin, Phys. Rev. D **51**, 6146 (1995).
[46] J. N. Bahcall, Phys. Rev. D **49**, 3923 (1994).
[47] J. M. Gelb and S. P. Rosen, hep-ph/9908325.
[48] B. Faïd, G. L. Fogli, E. Lisi and D. Montanino, Astropart. Phys. **10**, 93 (1999).
[49] First paper of Ref. [20].
[50] G. L. Fogli and E. Lisi, Astro. Part. Phys. **3**, 185 (1995).

[51] C. Arpesella *et al.*, BOREXINO proposal, Vols. 1 and 2, Ed. by G. Bellin et al. (University of Milano, Milano, 1991); R. S. Raghavan, Science **267**, 45 (1995); see also http://www.lngs.infn.it/site/exppro/borex/borexino.htm.
[52] A. Suzuki, for the KamLAND Collaboration, Nucl. Phys. (Proc. Suppl.) **77**, 171 (1999): see also http://www.awa.tohoku.ac.jp/html/KamLAND/index.html.
[53] V. Barger, R. J. N. Philips, and K. Whisnant, Phys. Rev. D **24**, 538 (1981).
[54] S. Pakvasa and J. Pantaleone, Phys. Rev. Lett. **65**, 2479 (1990).
[55] P. I. Krastev and S. T. Petcov, Nucl. Phys. B **449**, 605 (1996).
[56] See for *e.g.* , S. Geer, Phys. Rev. D **57**, 6989 (1998); *ibid.*, D **57**, 039903 (1999); A. De Rujula, M. B. Gavela, and P. Hernandez, Nucl. Phys. B **547**, 21 (1999). V. Barger. S. Geer, and K. Whisnant, Phys. Rev. D **61**, 053004 (2000).
[57] C. E. C. Lima and H. M. Portella, hep-ph/0005053.
[58] G. L. Fogli, E. Lisi, D. Montanino and A. Palazzo, hep-ph/0005261.

TABLES

TABLE I. Solar neutrino rates observed by Homestake, SAGE and GALLEX as well as theoretical predictions for the the Standard Solar Model by Bahcall and Pinsonneault [7]. For SK we show the ratio of the observed flux over the prediction of the BP98 SSM.

Experiment	Observed Rate	Ref.	BP98 SSM Predictions [7]	Units
Homestake	2.56 ± 0.21	[2]	$7.7^{+1.2}_{-1.0}$	SNU
SAGE	72.5 ± 5.5	[5]	129^{+8}_{-9}	SNU
GALLEX	72.5 ± 5.5	[4]	129^{+8}_{-9}	SNU
Super-Kamiokande	0.475 ± 0.015	[6]	$1.00^{+0.19}_{-0.14}$	5.15×10^6 cm^{-2}s^{-1}

TABLE II. The best fitted parameters and $\chi^2_{\rm min}$ as well as C.L. (in %) for the 2 generation LVO solution to the SNP. Numbers of degree of freedom ($N_{\rm DOF}$) are also indicated. The matter effect was taken into account unless it is indicated in parentheses. Note that for spectrum analysis matter effect was neglected, as it is a good approximation (see section II A, III B). We also present the values of the local best fit which explain better the total rates in the line indicated as Combined (R).

Case	$\Delta m^2_{12} \times 10^{10}$ eV^2	$\sin^2\theta_{12}$	$f_{\rm B}$	$\chi^2_{\rm min}$	$N_{\rm DOF}$	CL (%)
Rates	0.91	0.27/0.73	1 (fixed)	1.82	2	40.3
Spectrum	4.4	0.28/0.72	–	15.7	15	40.2
Combined (w/o matter)	4.4	0.37/0.63	1 (fixed)	31.9	24	12.9
Combined	4.4	0.37/0.63	1 (fixed)	31.3	24	14.5
Combined (R)	0.65	0.23/0.77	1 (fixed)	33.7	24	9.0
Rates	0.83	0.37/0.63	1.6	0.72	1	69.8
Combined (w/o matter)	4.4	0.34/0.66	0.77	30.3	23	14.1
Combined	4.4	0.35/0.65	0.78	29.8	23	15.5
Combined (R)	0.65	0.23/0.77	0.96	33.7	23	7.0

TABLE III. The best fitted parameters and $\chi^2_{\rm min}$ for the 3 generation LVO solution to the SNP.

Case	$\sin^2\theta_{13}$	$\Delta m^2_{12} \times 10^{10}$ eV^2	$\sin^2\theta_{12}$	$f_{\rm B}$	$\chi^2_{\rm min}$	$N_{\rm DOF}$	CL (%)
Rates	0.0	0.91	0.27/0.73	1 (fixed)	1.82	1	17.7
Spectrum	0.0	4.4	0.28/0.72	–	15.7	14	33.2
Combined	0.05	4.4	0.32/0.68	1 (fixed)	31.0	23	12.3
Combined (R)	0.05	0.65	0.2/0.8	1 (fixed)	33.2	23	7.8
Rates	0.0	0.83	0.37/0.63	1.6	0.72	0	–
Combined	0.05	4.4	0.29/0.71	0.79	29.8	22	12.3
Combined (R)	0.05	0.65	0.2/0.8	0.94	33.2	22	5.9

TABLE IV. The best fitted parameters and $\chi^2_{\rm min}$ for the 2 generation LVO solution to the SNP without the chlorine data.

Case	$\Delta m^2_{12} \times 10^{10}$ eV^2	$\sin^2\theta_{12}$	$f_{\rm B}$	$\chi^2_{\rm min}$	$N_{\rm DOF}$	CL (%)
Rates	0.91	0.25/0.75	1 (fixed)	0.71	1	39.9
Combined	4.4	0.34/0.66	1 (fixed)	25.2	23	34.0

TABLE V. The best fitted parameters and $\chi^2_{\rm min}$ for the 3 generation LVO solution to the SNP without the chlorine data.

Case	$\sin^2\theta_{13}$	$\Delta m^2_{12} \times 10^{10}$ eV^2	$\sin^2\theta_{12}$	$f_{\rm B}$	$\chi^2_{\rm min}$	$N_{\rm DOF}$	CL (%)
Rates	0.05	0.44	0.44/0.56	1 (fixed)	0.70	0	–
Combined	0.05	4.4	0.28/0.72	1 (fixed)	25.0	22	29.7

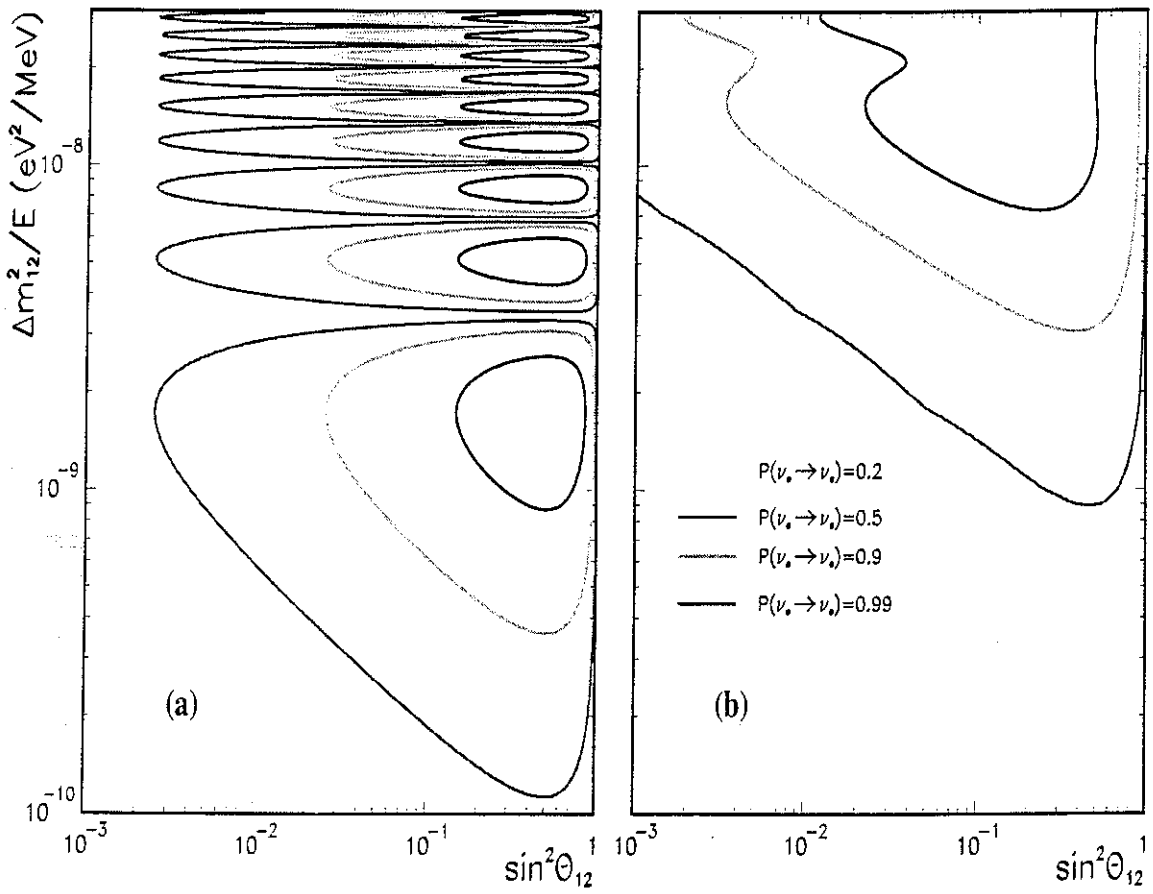

FIG. 1. Contours of iso-survival probability of ν_e at the surface of the Sun as a function of $\Delta m^2_{12}/E$ and $\sin^2\theta_{12}$ (a) considering pure vacuum oscillation, and (b) when matter is taken into account. For the case (b) we numerically integrated the evolution Eq. (1) assuming that neutrinos are created at the center of the Sun.

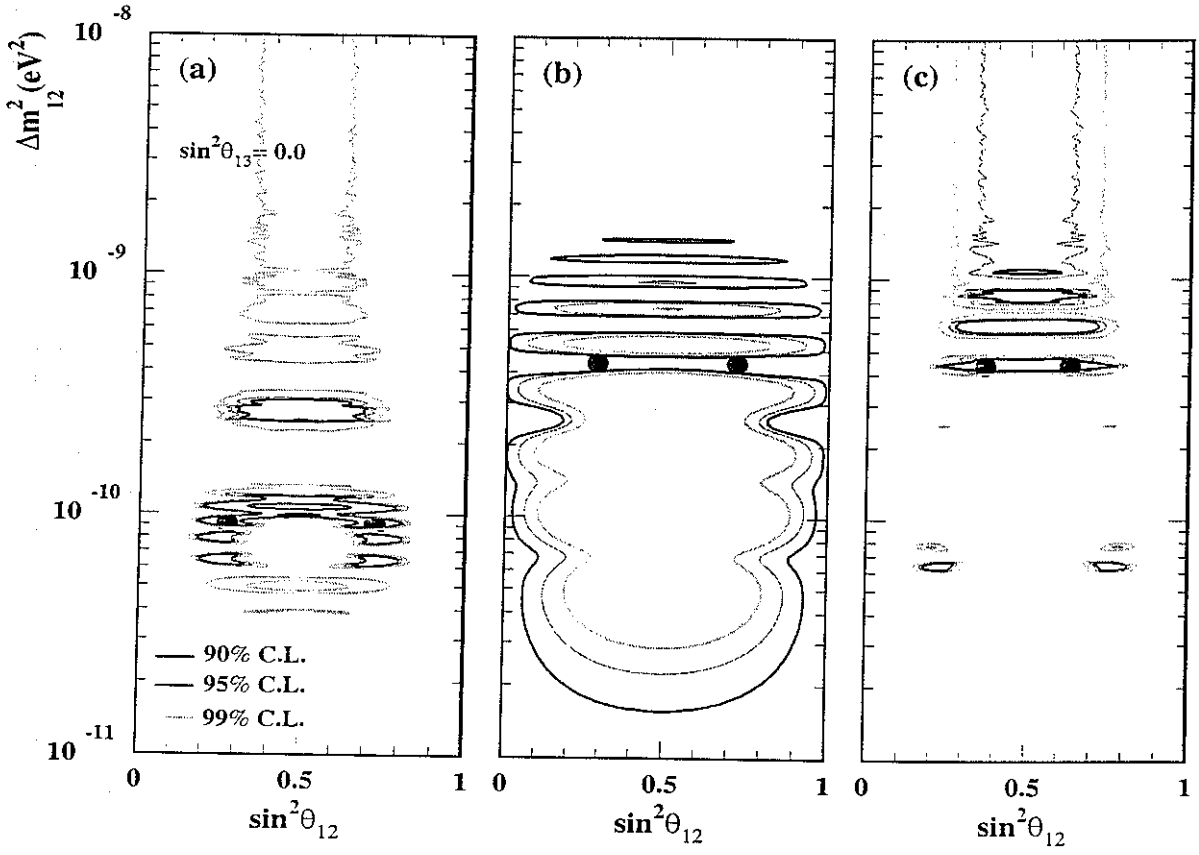

FIG. 2. Region of $(\sin^2\theta_{12}, \Delta m^2_{12})$ allowed by (a) the total rates from ^{37}Cl. ^{71}Ga and SK (b) the SK spectrum and (c) the combined analysis of Rates + SK Spectrum in the long-wavelength vacuum oscillation scenario for 2 neutrino flavors. The best fit points are shown as black circles. Solar matter effect is not taken into account.

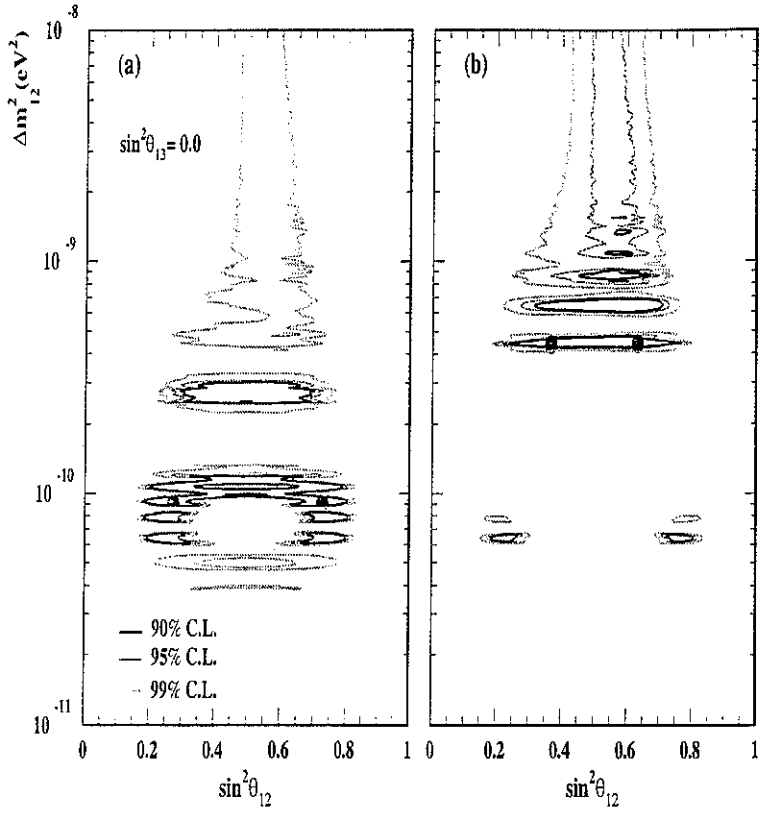

FIG. 3. Same as in Figs. 2 (a) and (c) but with the solar matter effect.

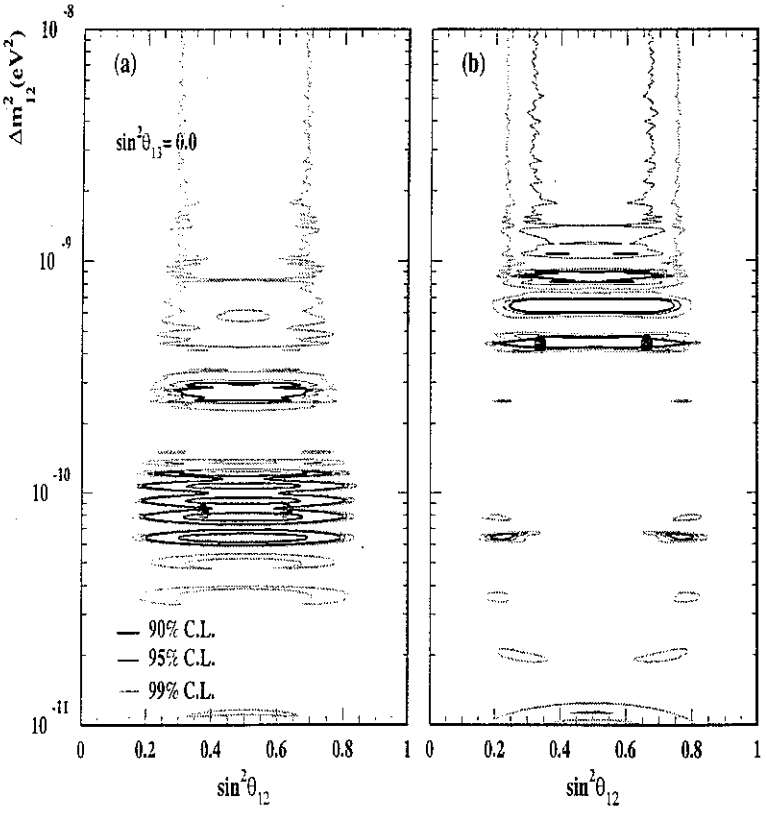

FIG. 4. Same as in Figs. 2 (a) and (c) but with arbitrary ^{8}B neutrino flux normalization f_B.

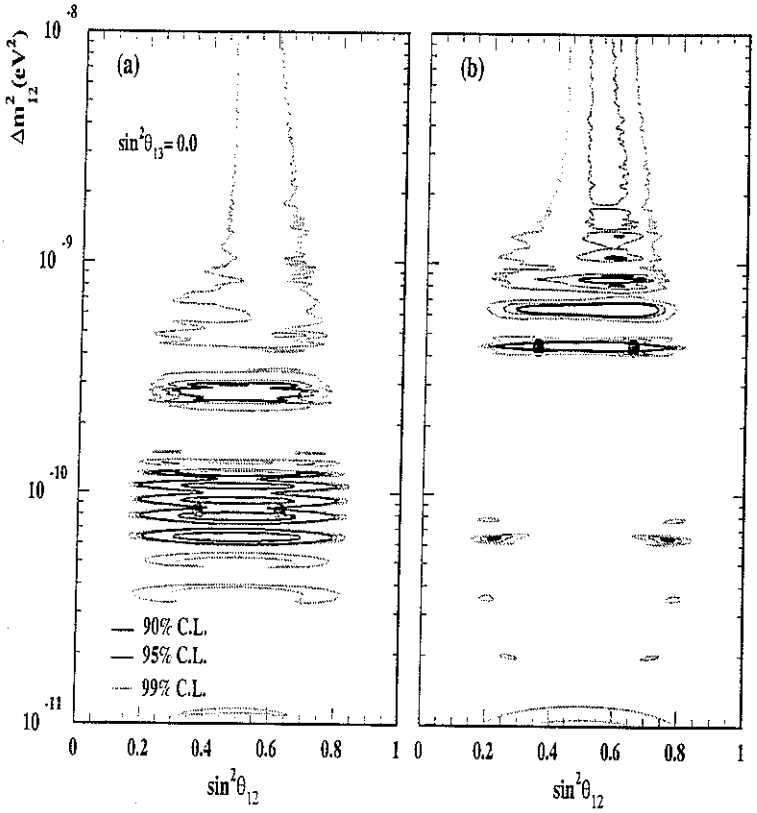

FIG. 5. Same as in Fig. 4 but with the MSW effect in the Sun.

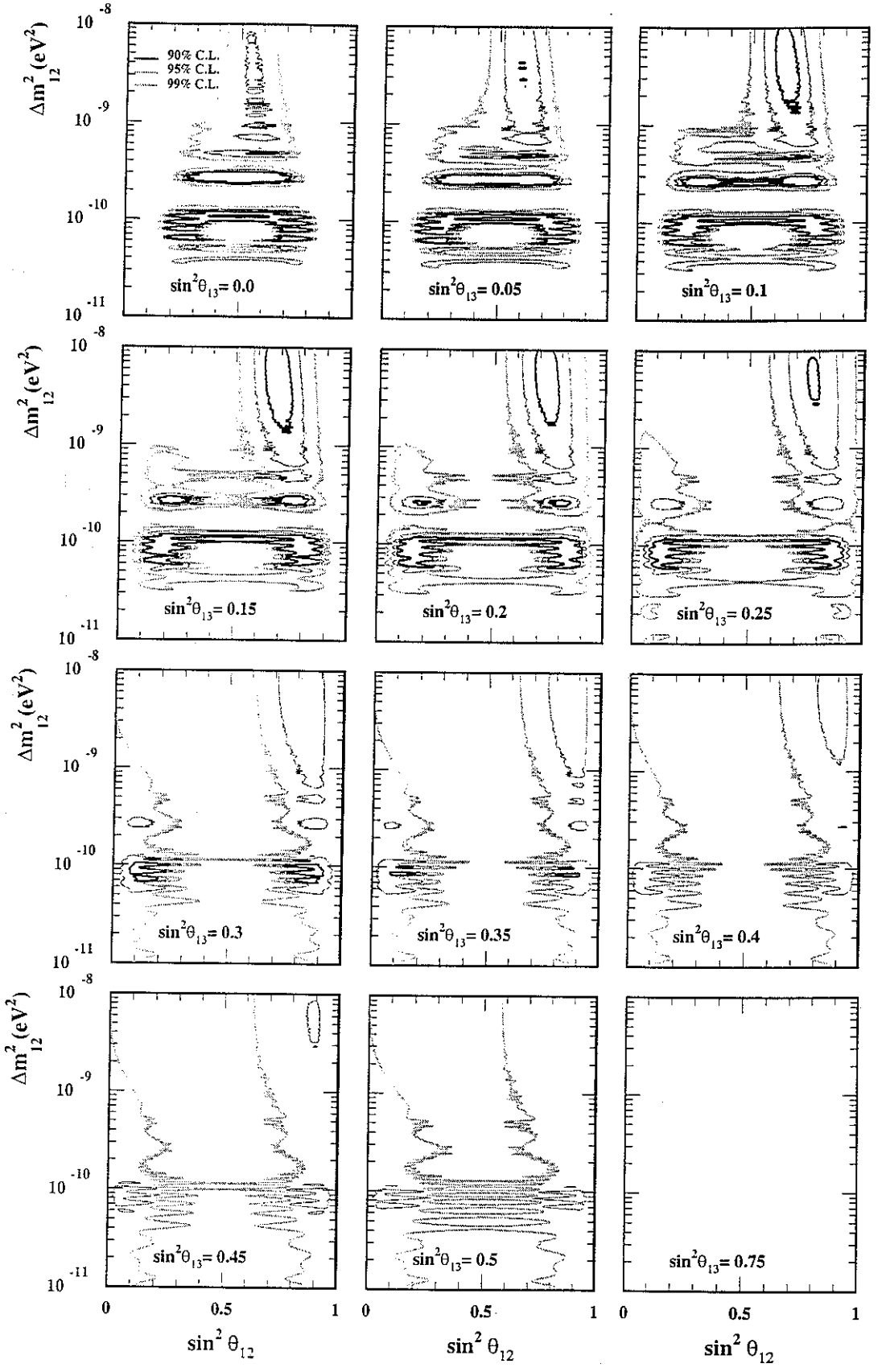

FIG. 6. Region of $(\sin^2\theta_{12}, \Delta m^2_{12})$ allowed by the total rates from ^{37}Cl, ^{71}Ga and SK for various values of $\sin^2\theta_{13}$ for the long-wavelength vacuum oscillation solution to the SNP with 3 neutrino flavors.

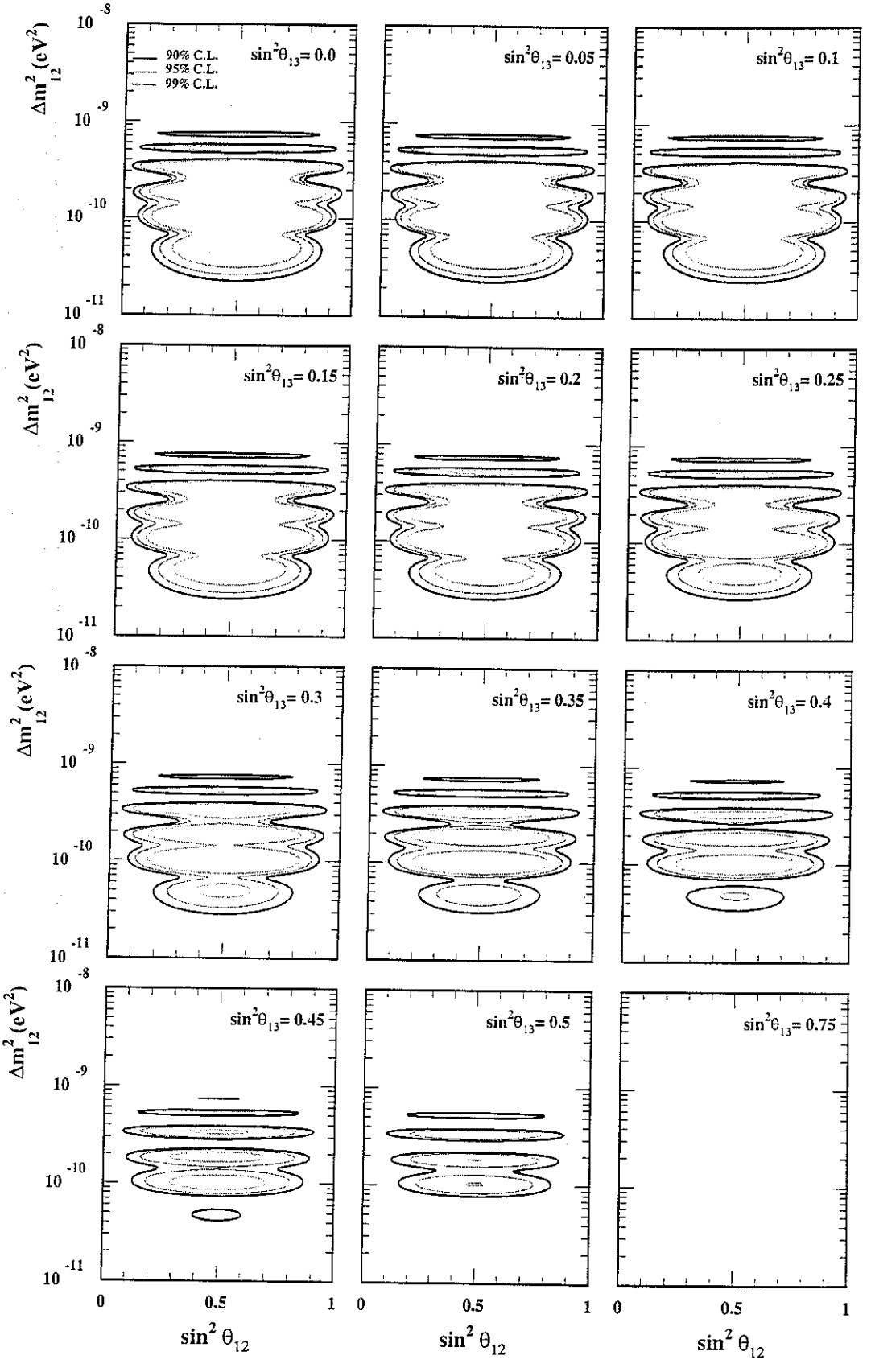

FIG. 7. Region of $(\sin^2\theta_{12}, \Delta m^2_{12})$ allowed by the SK spectrum for various values of $\sin^2\theta_{13}$ for the LVO solution to the SNP with 3 neutrino flavors.

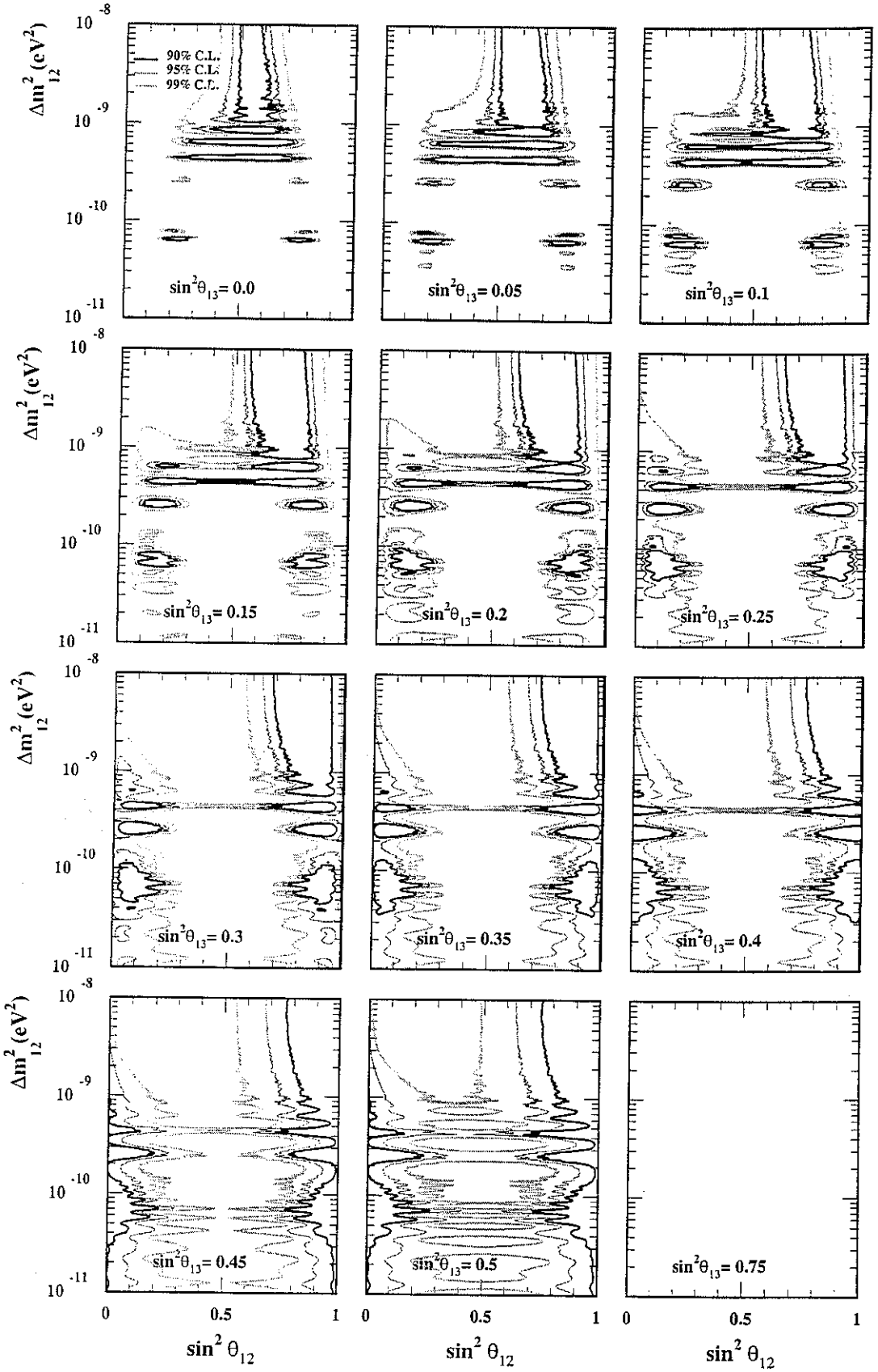

FIG. 8. Same as in Fig. 6 but for the combined analysis of total rates + SK spectrum.

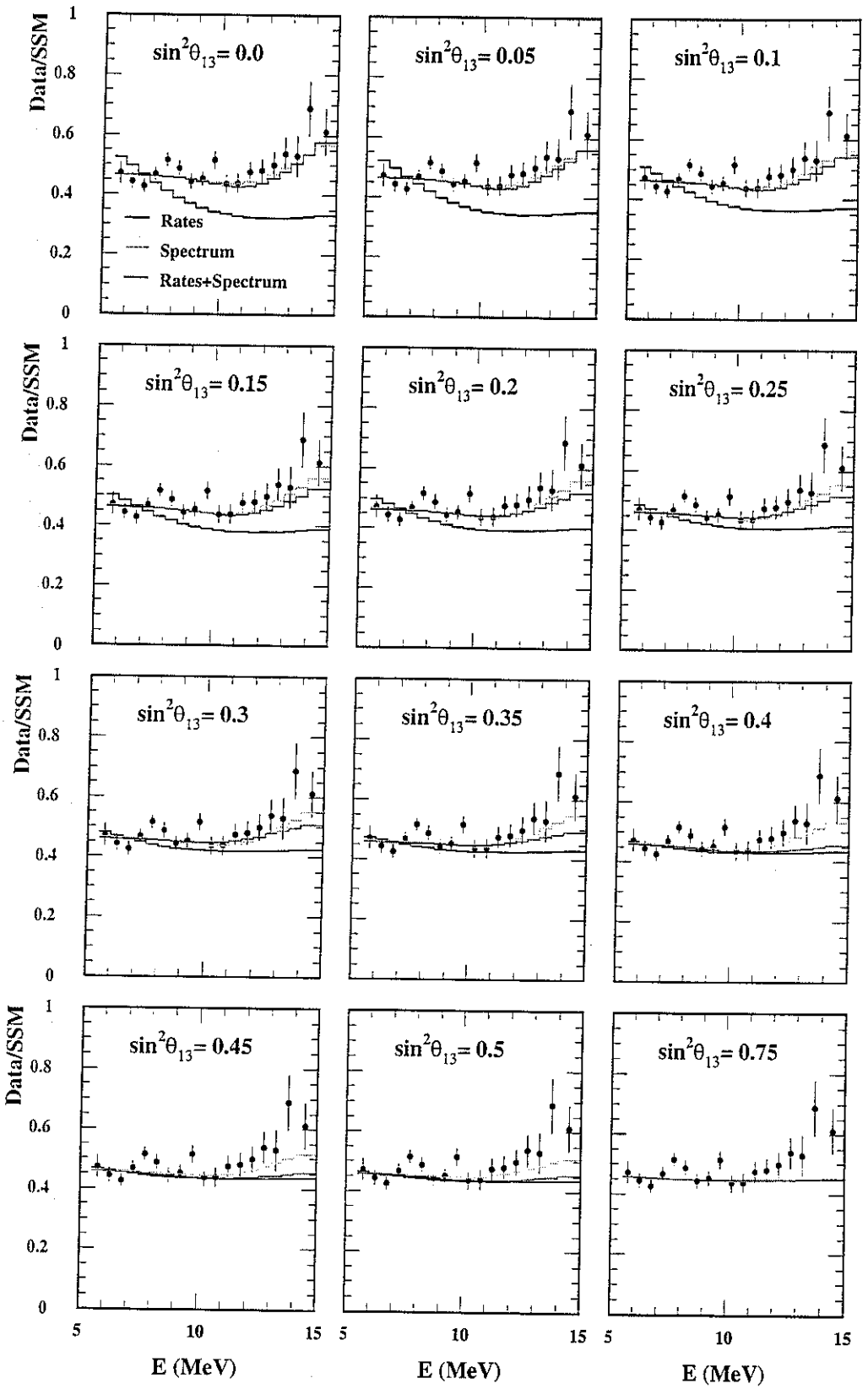

FIG. 9. Expected SK spectrum using the best fitted values of $(\sin^2\theta_{12}, \Delta m^2_{12})$. We note that the spectrum curves determined only by the rates are adjusted in such a way that χ^2 defined in Eq. (21) takes minimum values after we determine the values of $(\sin^2\theta_{12}, \Delta m^2_{12})$ by the fit only with the rates.

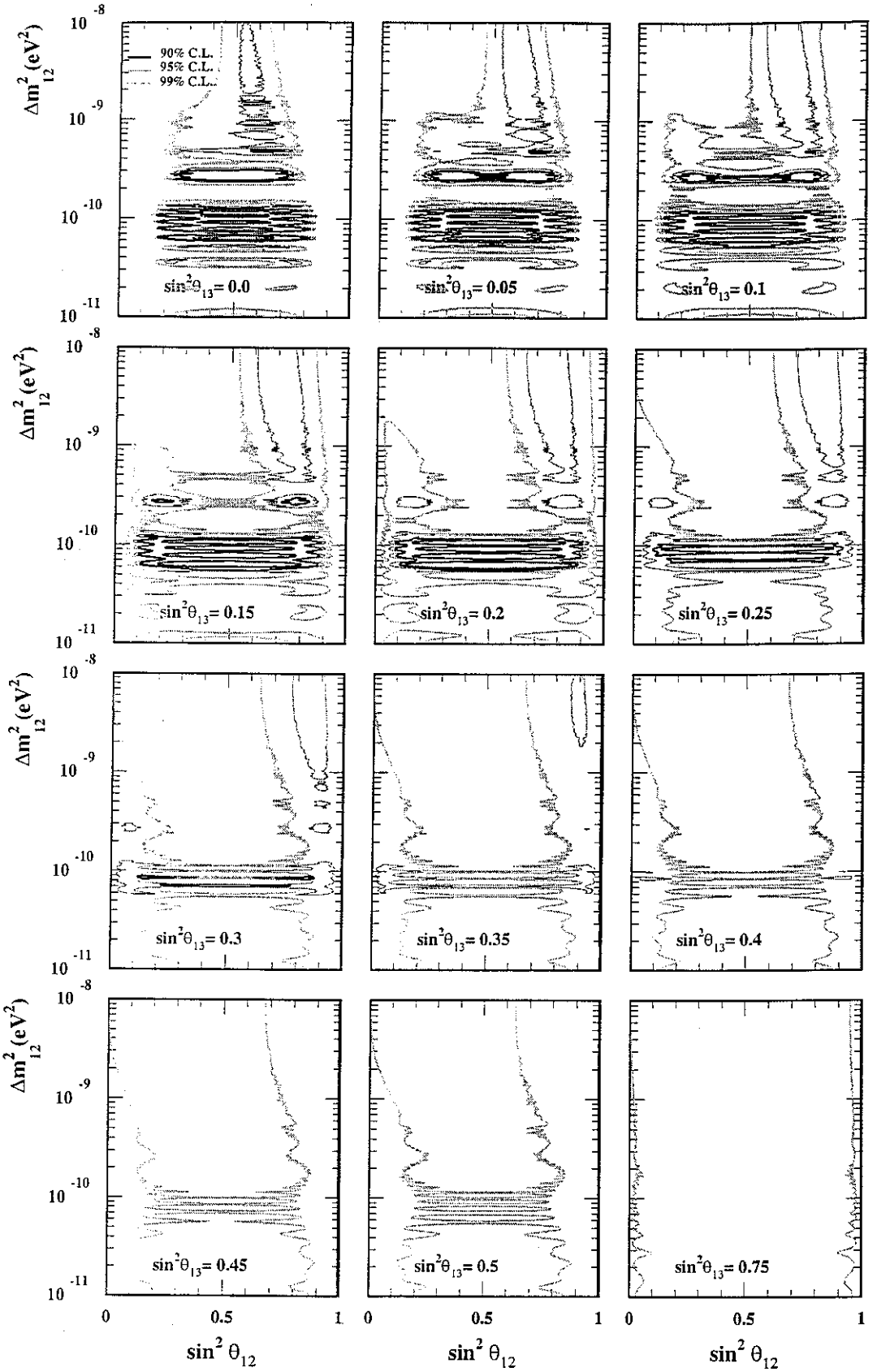

FIG. 10. Same as in Fig. 6 but with arbitrary ^{8}B neutrino flux normalization f_B.

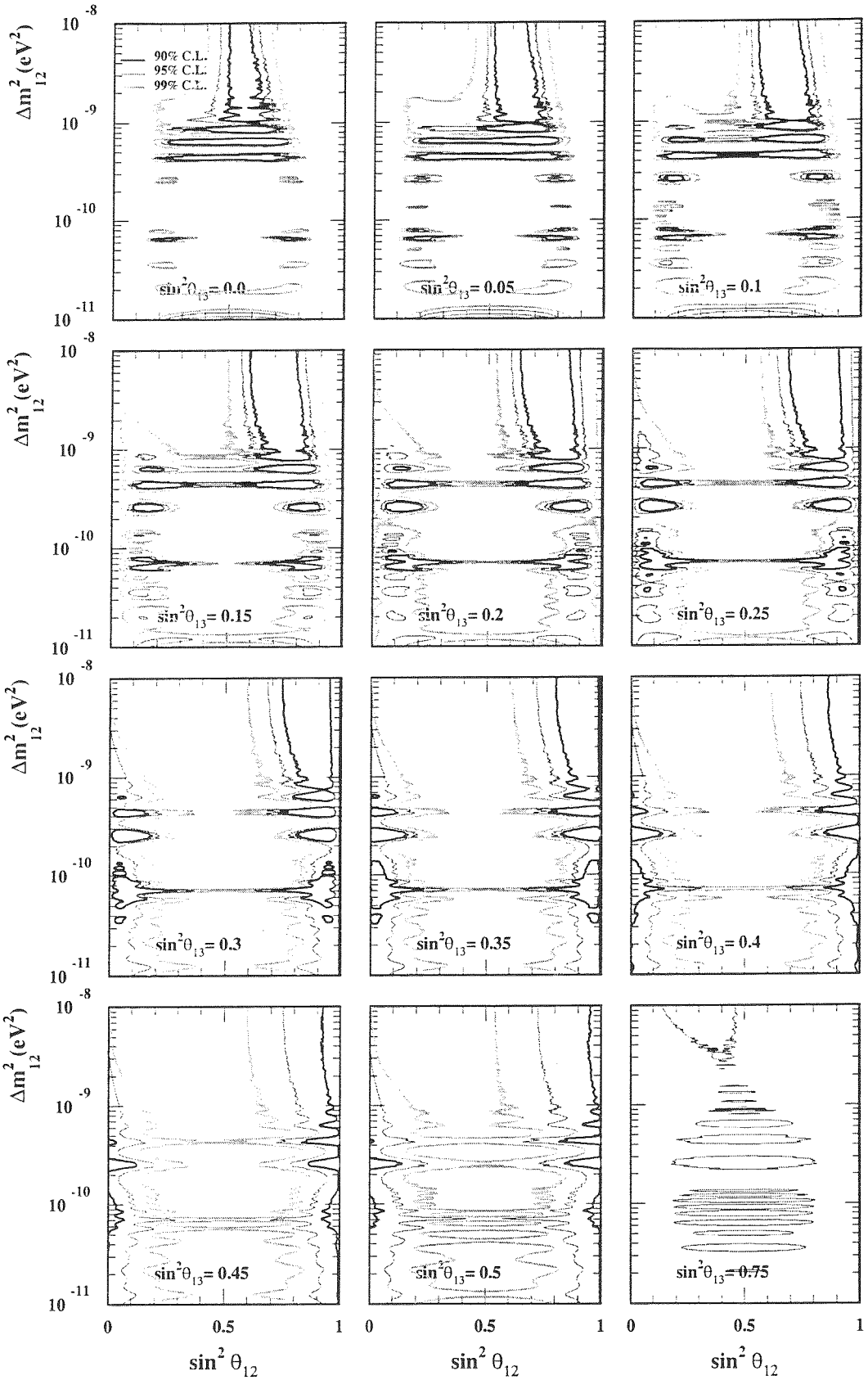

FIG. 11. Same as in Fig. 10 but for the combined analysis of total rates + SK spectrum.

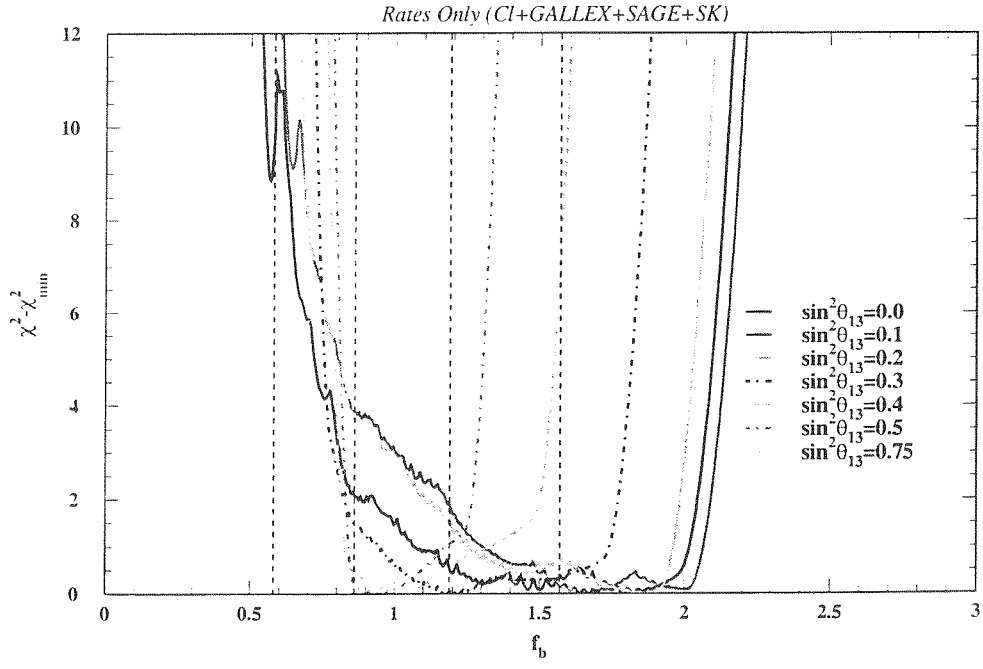

FIG. 12. $\chi^2 - \chi^2_{\rm min}$ is plotted as a function of $f_{\rm B}$ for various values of $\sin^2\theta_{13}$. We also show, by the vertical lines, the range of allowed values of $f_{\rm B}$ at one and three standard deviations as predicted by the BP98 SSM [7].

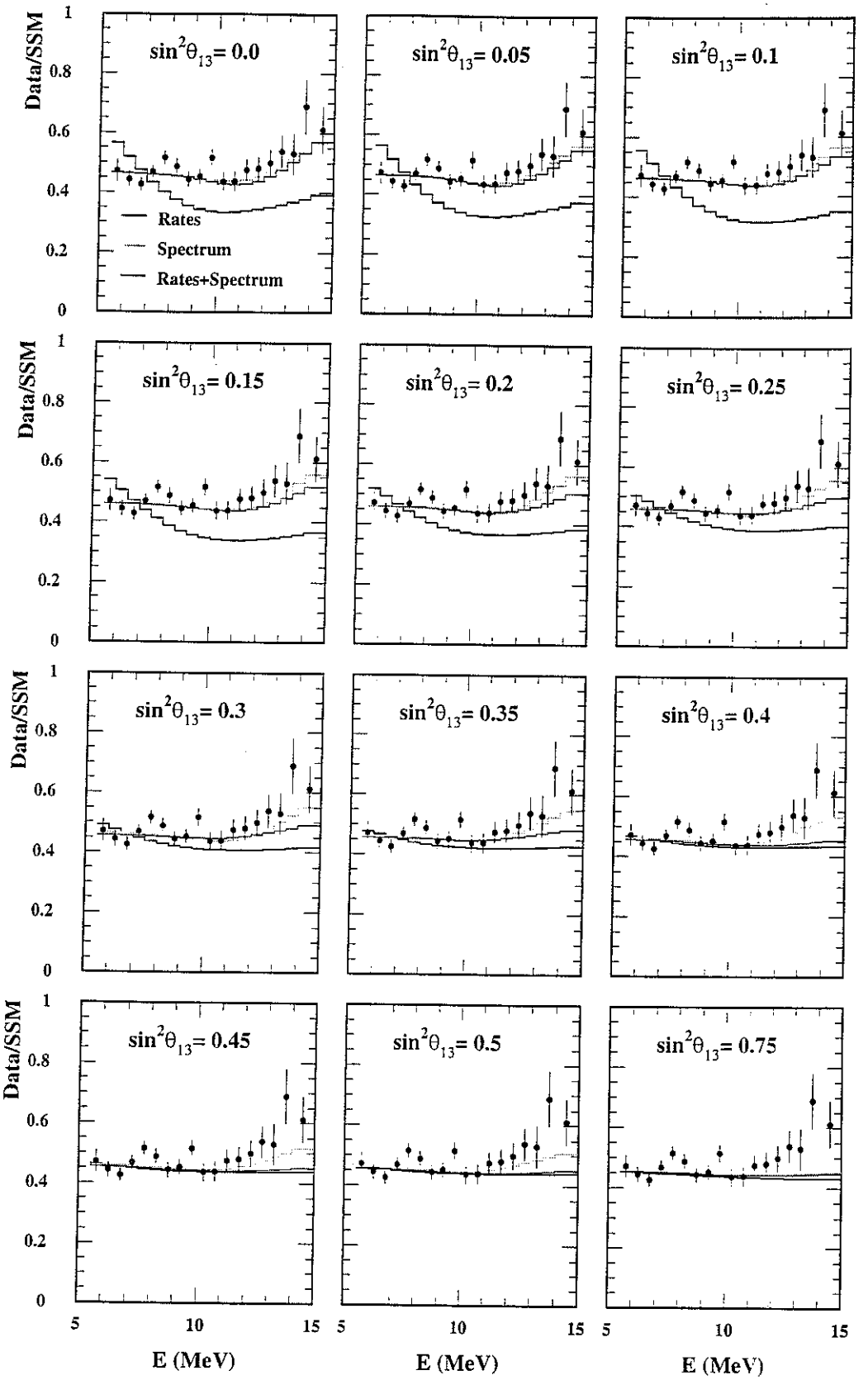

FIG. 13. Expected SK spectrum using the best fitted values of $(\sin^2\theta_{12}, \Delta m^2_{12})$ when considering f_B to be free.

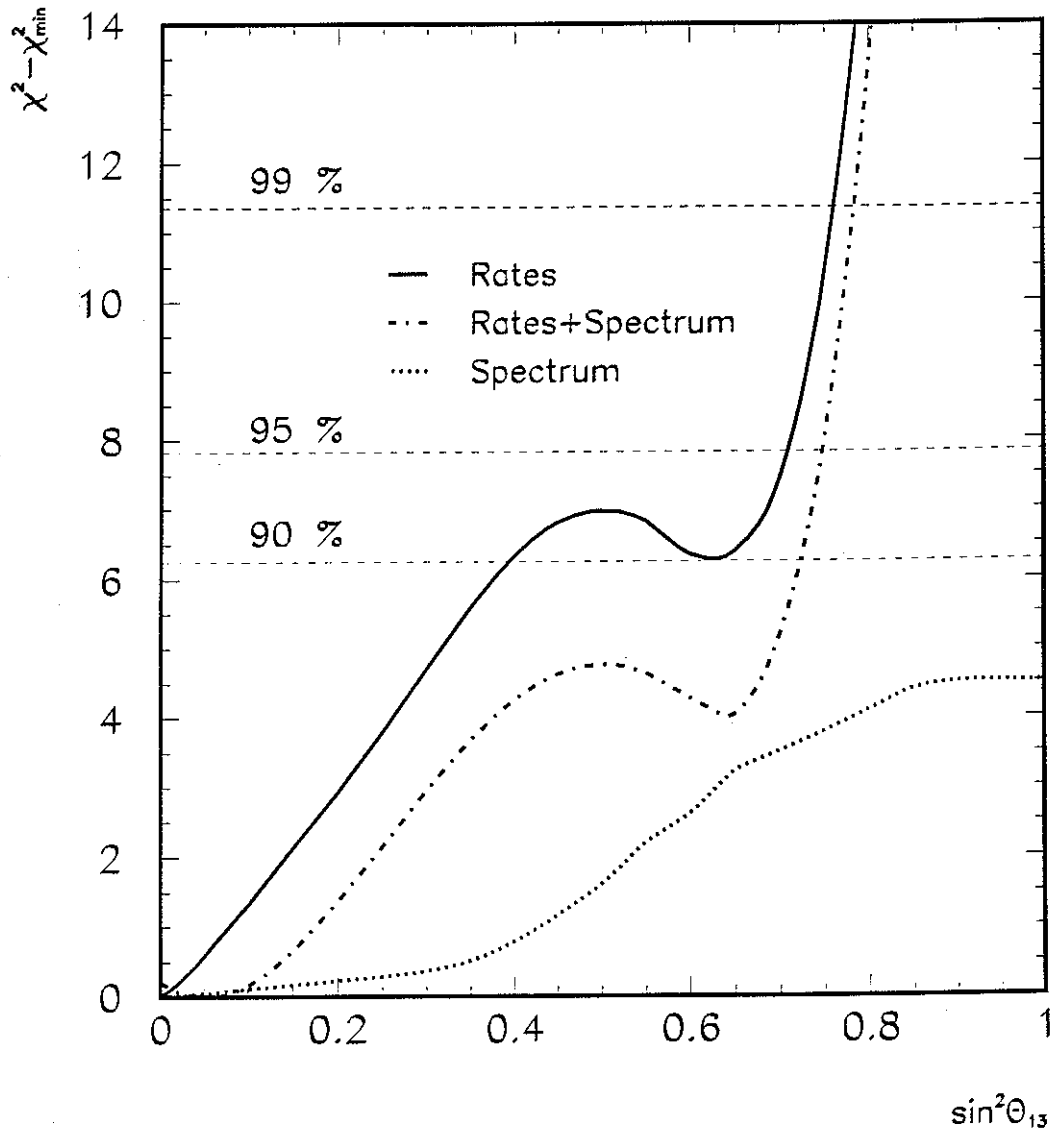

FIG. 14. $\chi^2 - \chi^2_{\rm min}$ as a function of $\sin^2\theta_{13}$, for the case when f_B is fixed to be 1.

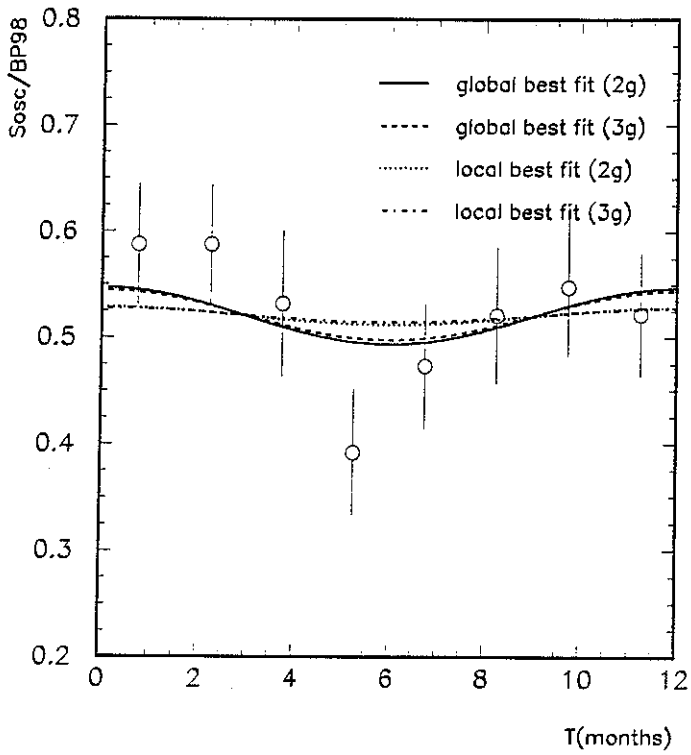

FIG. 15. Expected seasonal variation at SK for the best fitted parameters of the two and three generation LVO solutions to the SNP. We also show in the plot the experimental data points.

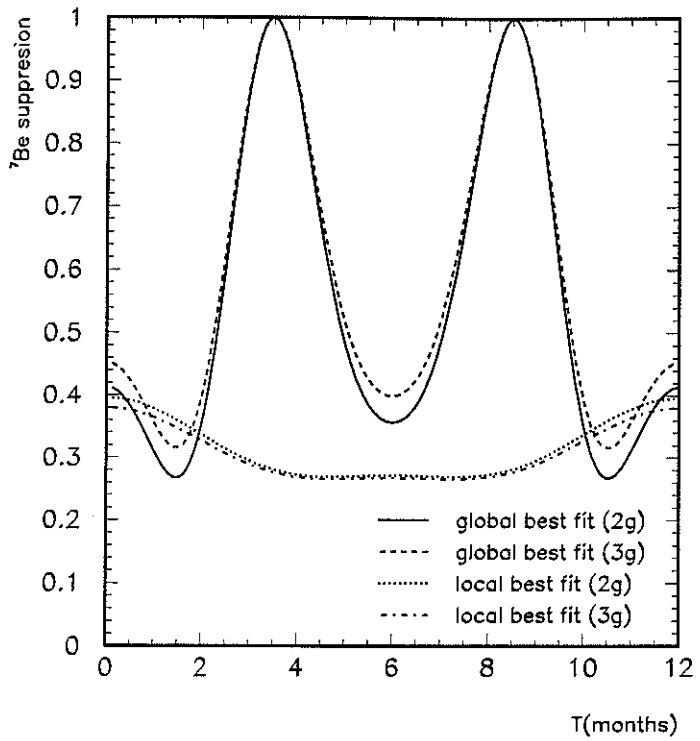

FIG. 16. Expected seasonal variation at Borexino and KamLAND for the best fitted parameters of the two and three generation LVO solutions to the SNP. We have subtracted the effect of the normal seasonal variation (due to $\sim 1/L^2$ dependence) expected in the absence of any oscillation.

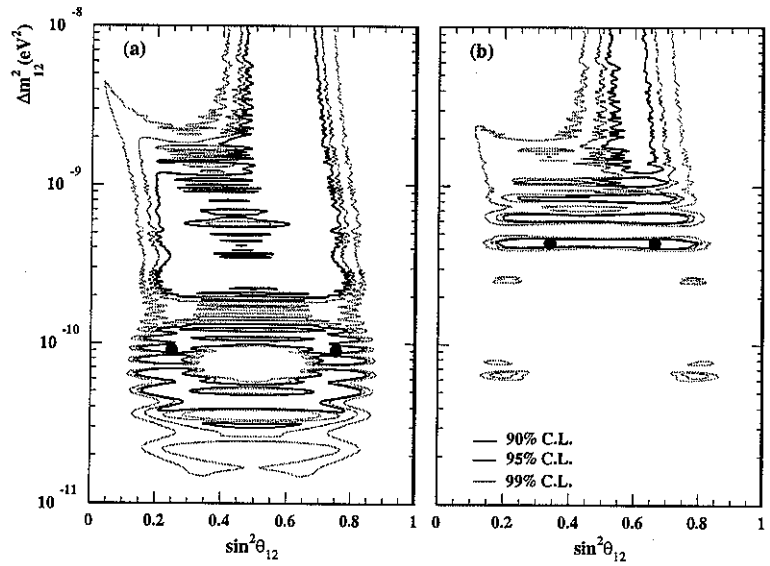

FIG. 17. Region of $(\sin^2\theta_{12}, \Delta m^2_{12})$ allowed by (a) the total rates from ^{71}Ga and SK, (b) the SK spectrum and (c) the combined analysis of rates + SK Spectrum in the LVO scenario for 2 neutrino flavors. The best fit points are shown as a dark circle. Here we have ignored the information from ^{37}Cl.

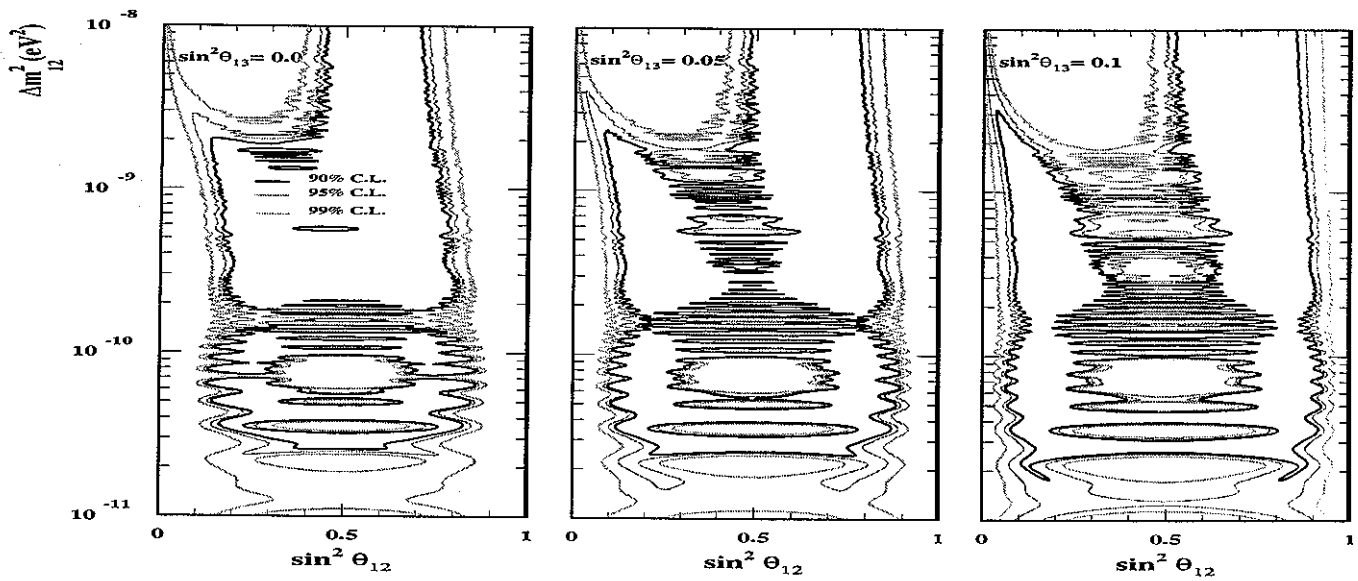

FIG. 18. Region of $(\sin^2\theta_{12}, \Delta m^2_{12})$ allowed by the total rates from ^{71}Ga and SK for various values of $\sin^2\theta_{13}$ for the LVO solution to the SNP with 3 neutrino flavors. Here we have ignored the information from ^{37}Cl.

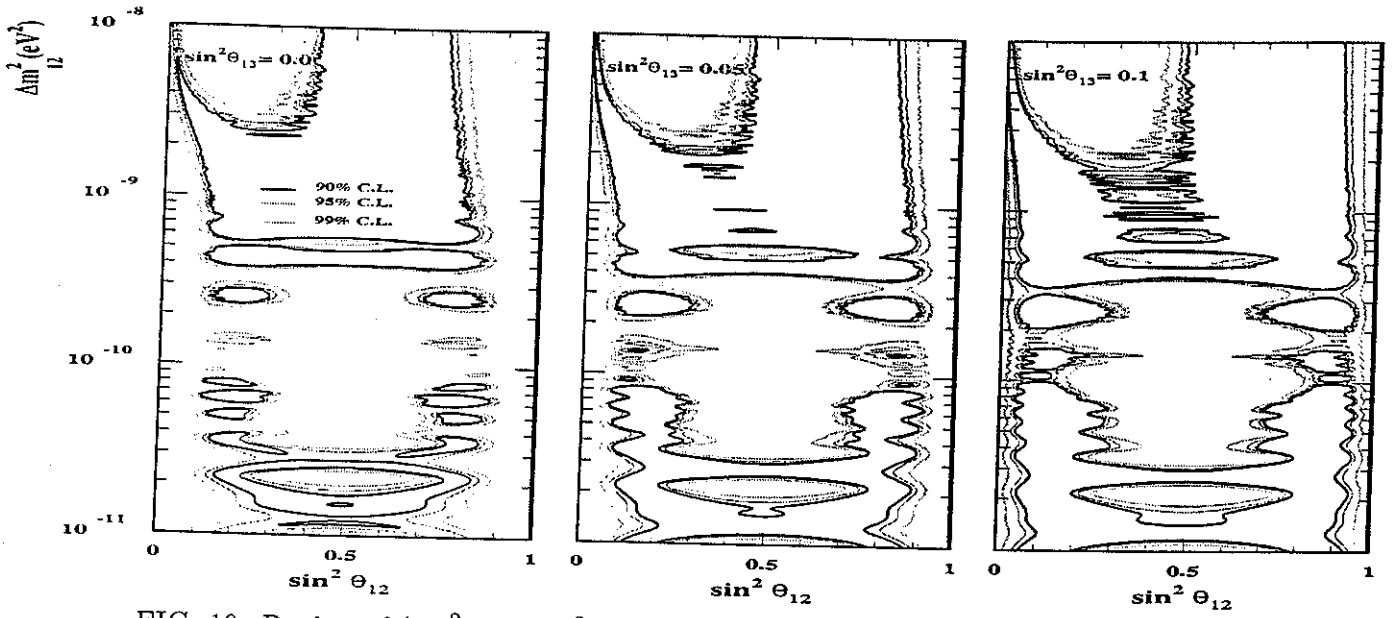

FIG. 19. Region of $(\sin^2\theta_{12}, \Delta m^2_{12})$ allowed by the combined analysis of rates + SK spectrum for various values of $\sin^2\theta_{13}$ for the LVO solution to the SNP with 3 neutrino flavors. Here we have ignored the information from ^{37}Cl.

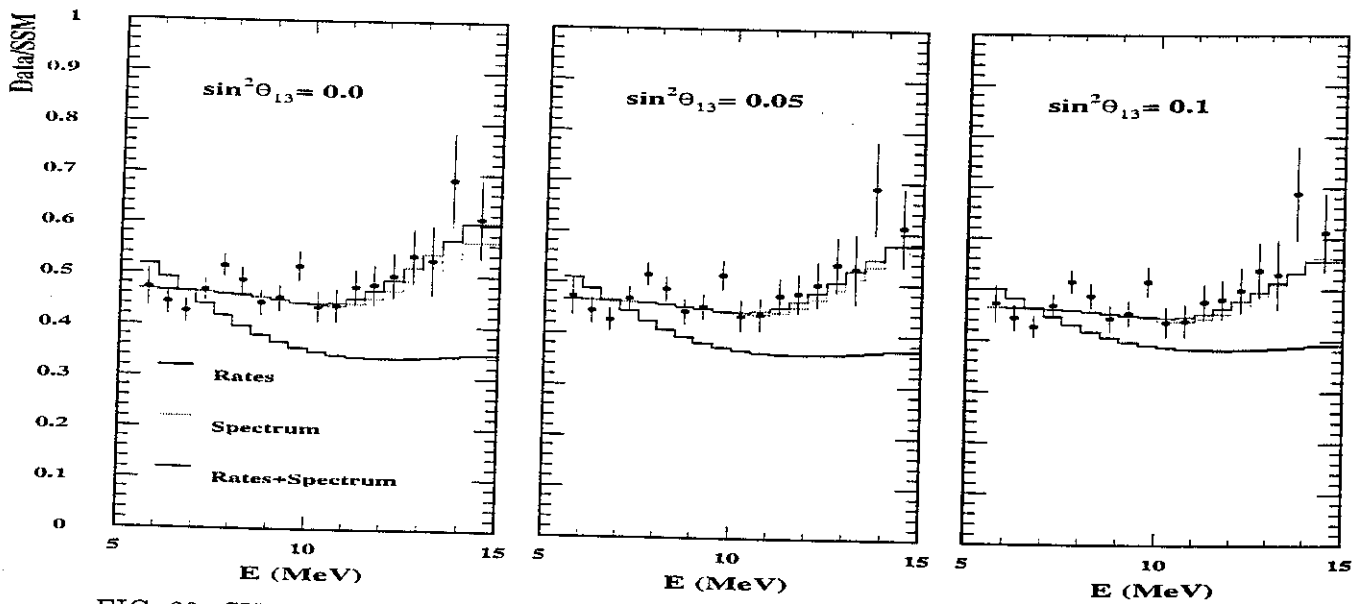

FIG. 20. SK spectrum for the best fitted values of rates and rates+SK spectrum combined for three values of $\sin^2\theta_{13}$. Here $f_B = 1$ and the total neutrino rate measured at Homestake is not taken into account.